Supplementary Information

A Crystalline Nitrogen Chain Radical Anion

Reece Lister-Roberts,[1,2] Daniel Galano,[1] Bono van IJzendoorn,[2] George F. S. Whitehead,[1] Adam Brookfield,[1,3] Alice M. Bowen,[1,3]* Nikolas Kaltsoyannis,[1]* Meera Mehta[2]*

Alice.Bowen@manchester.ac.uk, Nikolas.Kaltsoyannis@manchester.ac.uk, Meera.Mehta@chem.ox.ac.uk

1. Department of Chemistry, University of Manchester, Oxford Road, Manchester M13 9PL, U.K.

2. Department of Chemistry, University of Oxford, 12 Mansfield Road, Oxford OX1 3TA, U.K.

3. The EPSRC National Research Facility for Electron Paramagnetic Resonance, Photon Science Institute, University of Manchester, Oxford Road, Manchester, M13 9PL, U.K.

Table of Contents

1. Methods and Materials

1.1 Experimental Considerations

All manipulations were performed under an inert atmosphere using standard Schlenk line, and glovebox techniques. Glassware was flame dried prior to use.

Dry tetrahydrofuran (THF), diethyl ether (ether), toluene (Tol), dimethylformamide (DMF), hexane and pentane were obtained using Innovative Technologies anhydrous engineering solvent purification systems and subsequently degassed. 1,2-Difluorobenzene (*o*DFB) was dried over 3 Å molecular sieves. THF-d_8 and DMF-d_7 were dried over 3 Å sieves, $CDCl_3$ (containing TMS 1% v/v) and MeOD-D_4 were used without purification. All dry solvents were stored over activated 3 Å molecular sieves.

1-Azido-4-bromobenzene (4-$BrC_6H_4N_3$), 4-methylbenzenethiol (TolSH), triphenyltin hydride (Ph_3SnH), 4-iodobenzaldehyde (4-IC_6H_4CHO), cryptand-2.2.2, TEMPO, KCl, KH and cobaltocene were purchased from commercially available suppliers (Apollo Scientific, Sigma-Aldrich, Alfa Aesar, Fuorochem, Tokyo Chemical Industry, Thermo Fisher Scientific, and Acros Organics). KC_8 and Gomberg's dimer were synthesized using literature procedures.[1, 2]

1.2 Analytical Considerations

Nuclear Magnetic Resonance. ^{1}H, $^{13}C\{^{1}H\}$ and ^{119}Sn NMR were recorded on a Bruker AVIII 400 spectrometer using operating frequencies 400.17 MHz, 100.55 MHz and 149.24 MHz respectively. ^{1}H and $^{13}C\{^{1}H\}$ NMR chemical shifts were internally referenced to the residual solvent resonances (THF-d_8 (tetrahydrofuran-d_8): ^{1}H δ = 3.58, 1.73 ppm, $^{13}C\{^{1}H\}$ δ = 67.57, 25.37 ppm, ($CDCl_3$ (chloroform-d), MeOD-d_4 (methanol-d_4): ^{1}H δ = 4.78, 3.31 ppm, $^{13}C\{^{1}H\}$ δ = 49.15 ppm, ^{1}H δ = 7.26 ppm), DMF-d_7 (dimethylformamide-d_7): ^{1}H δ = 8.03, 2.92 ppm. ^{119}Sn chemical shifts were referenced externally to Me_4Sn. Solution phase NMR samples were prepared in 5 mm J Young NMR tubes (under an inert atmosphere) where stated. All NMR were analyzed using MestReNova V15.0.0 software

Ultraviolet–visible spectroscopy. Ultraviolet-visible (UV-Vis) electronic absorption spectra were recorded on a Mettler Toledo UV5Bio spectrophotometer using 10 mm path length quartz J Young cuvettes.

Electron Paramagnetic Resonance. Electron paramagnetic resonance (EPR) spectra were recorded at X band (9.4 GHz) with a Bruker EMXmicro spectrometer at 298 K. Spin counting was conducted on a Bruker Magnettech ESR5000 at X band (9.8 GHz), 298 K and analyzed

using the ESR Studio software's incorporated spin counting function. All EPR spectra were plotted using MATLAB R2024a and simulations conducted using easyspin-6.0.2 plugin.[3]

Superconducting quantum interference device: Magnetic measurements were made using a Quantum Design MPMS3 superconducting quantum interference device (SQUID) magnetometer. The sample was prepared by loading the crystalline solid into a gelatine capsule under an inert atmosphere.

Cyclic Voltammetry. Cyclic voltammetry (CV) was carried out in the glovebox under inert conditions with EMStat4s. Electrodes: Working – glassy carbon. Counter – platinum wire. Pseudo reference – silver wire. Reference – Ag /AgCl (leak proof).

Mass spectrometry. Mass spectrometry samples were analyzed by the mass spectrometry service at the University of Oxford using an electrospray ionization (ESI) equipped Waters RDa bench-top time of flight mass spectrometer. Samples were prepared under a nitrogen atmosphere and directly injected into the ionization source of the mass spectrometer.

Infrared spectroscopy. ATR-IR spectra were recorded on microcrystalline powders using a Bruker Alpha II under an inert atmosphere.

Elemental analysis. Elemental analysis was carried out by the microanalysis service of the University of Manchester using a Flash 2000 elemental analyser. Samples were prepared under a nitrogen atmosphere.

X-ray diffraction studies. X-ray diffraction data was collected for compound [K(crypt)][**1**] on a dual source Rigaku FR-X rotating anode at 100K with Cu Kα (1.54184 Å) radiation, equipped with a Hypix000HE detector and Oxford cryosystem. X-ray diffraction data was collected for all other compounds on an Oxford Diffraction Supernova dual-source diffractometer at 150K using Cu Kα (1.54184 Å) radiation equipped with a 135 mm Atlas CCD area detector. X-ray data was collected using CrysAlisPro software.[4]

Crystal structure determination and refinements: X-ray data was processed and reduced using CrysAlisPro. Absorption correction was performed using empirical methods (SCALE3 ABSPACK) based upon symmetry-equivalent reflections combined with measurements at different azimuthal angles. The crystal structure was solved and refined against all F2 values using the SHELX and Olex2 suite of programmes.[5, 6] All atoms were refined anisotropically. Hydrogen atoms were placed in calculated positions and refined using idealized geometries and assigned fixed isotropic displacement parameters.

The disordered [**1**] moiety in [K(crypt)][**1**] was modelled over two positions and atomic displacement parameters were restrained to be similar using SHELX SIMU and SADI commands. In $[K(THF)_2]_2$[**2**] the atomic displacement parameters were restrained to be similar using SHELX SIMU, RIGU and SADI commands.

Crystallographic data have been deposited with the CCDC (CCDC 2423978-2423981).

Powder X-ray diffraction: Data collection. Microcrystalline sample of [K(crypt)][**1**] was sealed inside a 0.5 mm outer diameter capillary and data were collected using a Rigaku FR-X rotating anode single crystal X-ray diffractometer using Cu Kα radiation (λ = 1.5418 Å) with a Hypix-6000HE detector and an Oxford Cryosystems nitrogen flow gas system. Data were collected between 3–50 ° 2θ with a detector distance of 150 mm and a beam divergence of 0.5 mRad.[7] X-ray data were collected using CrysAlisPro software.[4]

Data processing. The instrument was calibrated using the collected data, with the instrument model refined using diffraction peak positions measured at multiple detector angles. X- ray data were reduced and integrated using CrysAlisPro software.[4] Peak hunting and unit cell indexing was performed using TOPAS software.[8] Le Bail profile analysis was performed using JANA2020 software.[9]

1.3 General Computational Considerations:

DFT geometry optimizations and frequency calculations were carried out using the Gaussian 16 package, revision C.01.[10] Following benchmarking studies (see Section 2.3) the Tao–Perdew–Staroverov–Scuseria (TPSS) functional was used. Geometry optimizations were performed, with default settings, starting from crystallographic co-ordinates. Analysis of the harmonic vibrational frequencies confirmed the optimized geometries as energetic minima. IR spectra were plotted using the calculated vibrational frequencies (Figure S21 and S22). Grimme's quasi-harmonic correction was employed to obtain the Gibbs free energies, using the python-based code GoodVibes.[11, 12, 13] The Ahlrichs Def2 basis set of polarized triple-ζ quality (Def2-TZVP) was used for all atoms.[14] Solvent environment was modelled using the smd method, with parameters appropriate to THF and cyclopentanone (a suitable model for *o*DFB).[15] Natural bond orbital (NBO) and natural resonance theory (NRT) calculations were carried out using NBO 7.0 program.[16] Mulliken and Hirshfeld charges and spin densities were computed.

50 state, full TDDFT calculations were performed using the Gaussian 16 package with the meta-hybrid TPSS (TPSSh) functional (following benchmarking, see Section 2.14.2).[17] The Def2-TZVP basis set was used for all atoms.

EPR calculations were carried out using ORCA 5.0.4 with the B3LYP functional.[18, 19, 20] Dunning's correlation consistent basis set of polarized triple-ζ quality with diffuse functions (aug-cc-pVTZ) was used for Br, with Barone's EPR-III basis set for all other atoms.[21, 22] Löwdin charges and spin densities were also obtained from a single point calculation carried out within ORCA 5.0.4 at the TPSS/Def2-TZVP level of theory. Solvent environment was modelled using the smd method, with parameters appropriate to THF.

2. Synthesis and Characterization

2.1 Synthesis of literature known compounds

2.1.1 Preparation of Potassium Graphite (KC_8)[2]

Freshly cut potassium (1 g, 25.6 mmol, 1 equiv.) and graphite (2.46 g, 204.8 mmol, 8 equiv.) were added to an ampoule in the glovebox and then heated under static vacuum at 130 °C for three hours with regular shaking. Potassium graphite was formed as a golden-brown powder in quantitative yield and used without further purification.

Isolated Yield: 3.46 g (>99%)

2.1.2 Preparation of Gomberg's Dimer[1]

In an ampoule wrapped in tin foil, zinc powder (1.7 g, 26.0 mmol, 5.2 equiv.) was added to a solution of triphenylmethyl chloride (1.4 g, 5.0 mmol, 1 equiv.) in toluene and stirred for five days at room temperature. The yellow solution was filtered and solvent removed under reduced pressure to yield a light-yellow solid. The light-yellow solid was dried under vacuum for two days.

Isolated Yield: 0.94 g (70%)

^{1}H NMR (400 MHz, 298 K, THF-d_8): δ= 6.90-7.56 (m, 25H, aryl CH), 6.23 (m, 2H vinylic), 5.98 (m, 2H, vinylic), 5.21 (m, 1H, allylic).

2.2. Synthesis and Characterization Data of [K(crypt)][1]

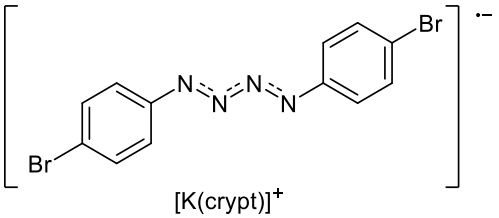

In the glovebox, KC_8 (10 mg, 0.074 mmol, 1 equiv.) and 2.2.2-cryptand (crypt; 28 mg, 0.074 mmol, 1 equiv.) were suspended in THF in a vial. 4-$BrC_6H_4N_3$ (19 uL, 0.148 mmol, 2 equiv.) was added and the vial shaken for 30 seconds. The solution was filtered and ether added to precipitate a black solid. The solid was filtered and washed with ether before drying under vacuum yielding [K(crypt)][**1**] as a black crystalline solid. Single crystals were obtained by slow vapour diffusion of hexane into THF at –40 °C. A mortar and pestle were used to grind the crystalline powder to a fine powder in the glovebox for use in powder x-ray diffraction studies.

Isolated Yield: 38.3 mg, 66%

At 15 x scale (2.22 mmol) Isolated Yield = 57%

At 30 x scale (4.44 mmol) Isolated Yield = 44%

Mass Spectrometry[23]: [[**1**]+H]$^-$ Found 366.9208 Calculated 366.9199

Elemental Analysis for $C_{34}H_{54}Br_2KN_6O_7$ [K(crypt)][1]•Et_2O: Expected: 47.61, 6.35, 9.80 Found: 47.44, 6.10, 9.68

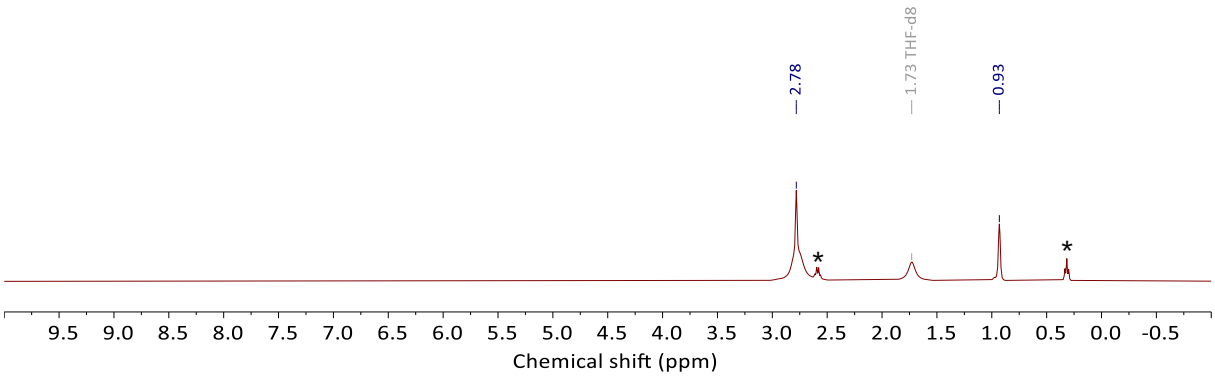

Figure S1: ^{1}H NMR spectrum (400 MHz, THF-d_8) of [K(crypt)][**1**]. Broadened K(crypt) signals due to presence of paramagnetic [**1**]$^{\bullet-}$. Residual ether solvent identified with *.

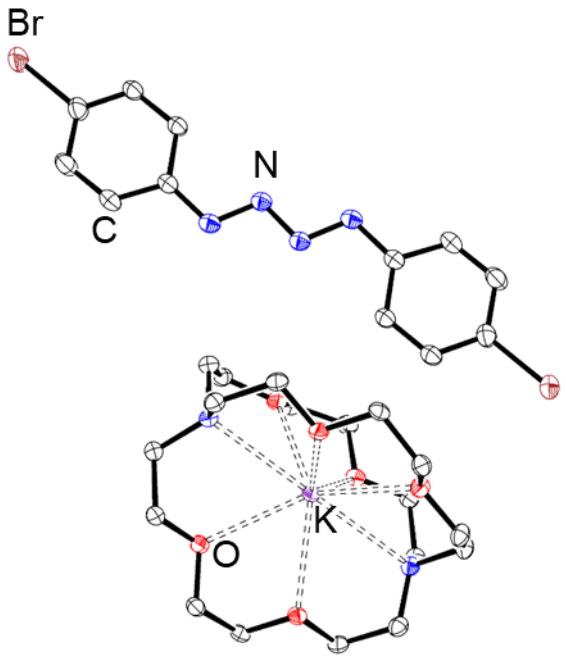

Figure S2: Molecular structure of [K(crypt)][**1**] showing anisotropic displacement ellipsoids at 50% probability. Hydrogen atoms omitted for clarity. Positional disorder omitted for clarity and major component (*ca.* 90% occupancy) shown. Nitrogen: blue; carbon: white; bromine: brown; potassium: violet; oxygen: red.

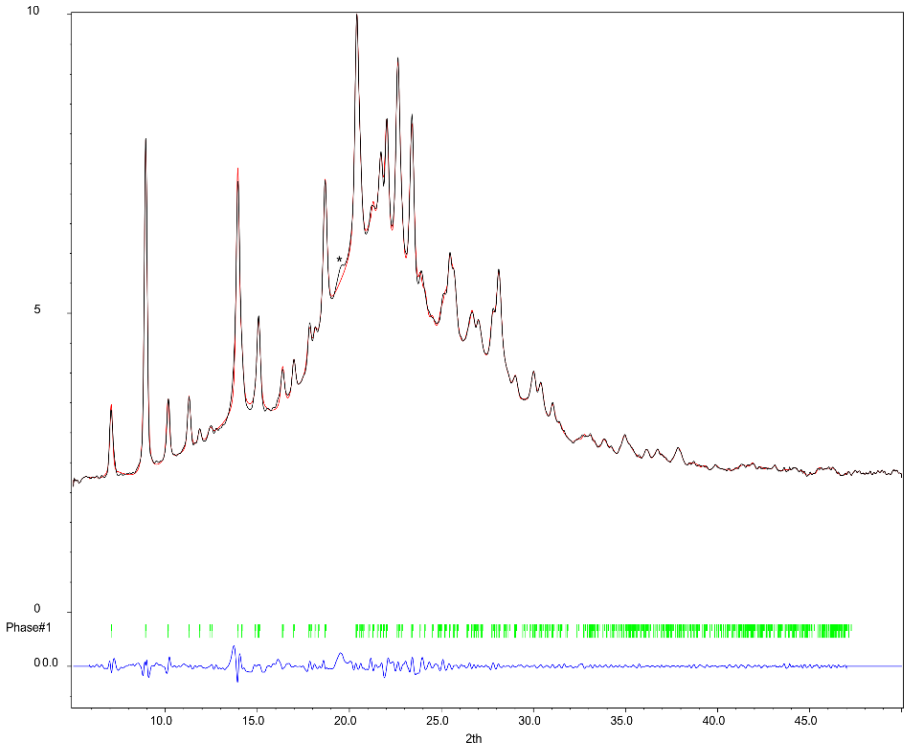

Figure S3: Experimental (black) and simulated (red) powder x-ray diffraction (PXRD) patterns of [K(crypt)][**1**] (minor impurity highlighted with *).

2.3 Functional benchmarking against geometric structure

Table S1: Experimental and calculated selected bond lengths for [**1**]$^{\bullet-}$ for a variety of functionals.[24, 25, 26]

Method	**N1A–N2A**	**N2A–N2B**	**N1B–N2B**
Experimental	1.324(8)	1.37(2)	1.324(8)
PBE	1.314	1.329	1.314
PBE0	1.297	1.307	1.297
TPSS	1.318	1.329	1.318
TPSSh	1.310	1.319	1.310
ωB97XD	1.297	1.308	1.297

2.4 Calculated Bond Metric Data

Table S2: Experimental and calculated selected bond lengths of [**1**]$^{\bullet-}$ with varying solvents/counterions at the TPSS/Def2-TZVP level.

Structure/Solvent	**N1A–N2A**	**N2A–N2B**	**N1B–N2B**
Experimental	1.324(8)	1.37(2)	1.324(8)
[**1**]$^{\bullet-}$/Gas Phase	1.318	1.329	1.318
[**1**]$^{\bullet-}$ /THF	1.319	1.329	1.319
[K(crypt)][**1**] /THF	1.318	1.330	1.318
[**1**]$^{\bullet-}$ /cyclopentanone	1.319	1.330	1.319
[K(crypt)][**1**] /cyclopentanone	1.318	1.330	1.318

Table S3: Calculated Wiberg Bond Order (WBI) for [**1**]$^{\bullet-}$ (no counterion) at the TPSS/Def2-TZVP level.

Solvent	N1A–N2A	N2A–N2B	N1B–N2B
THF	1.430	1.386	1.430
Cyclopentanone	1.428	1.386	1.428

It was found that the addition of the counter ion [K(Crypt)]$^{+}$ and choice of solvent had no significant impact on the optimized geometry.

2.5 Charge Delocalization Data

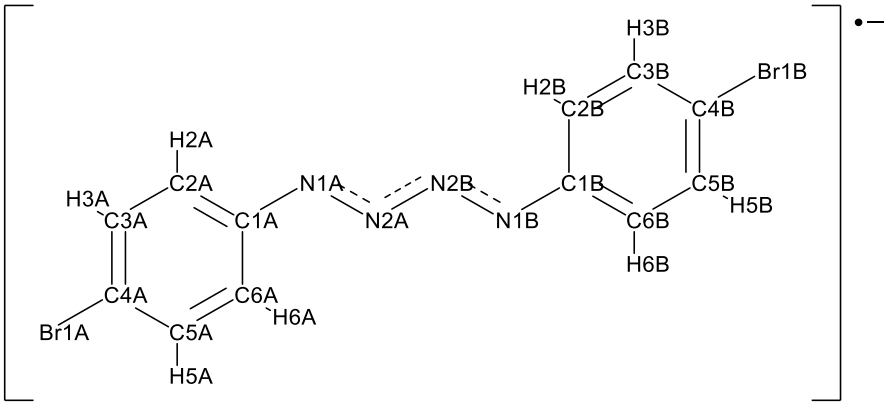

Table S4: Calculated NBO, Hirshfeld, Löwdin, and Mulliken charge distributions for [**1**]$^{\bullet-}$.

Atom	**Charge Distribution**			
	NBO	**Hirshfeld**	**Löwdin**	**Mulliken**
Br1A	0.000	-0.087	0.281	-0.172
N1A	-0.287	-0.199	-0.035	-0.088
N2A	-0.107	-0.127	-0.110	-0.167
C2A	-0.166	-0.060	-0.127	-0.228
H2A	0.117	0.030	0.144	0.096
C3A	-0.100	-0.054	-0.160	-0.191
H3A	0.112	0.045	0.150	0.135
C4A	-0.103	-0.019	-0.385	0.176
C5A	-0.106	-0.057	-0.162	-0.177
H5A	0.113	0.045	0.151	0.132
C6A	-0.143	-0.056	-0.118	-0.229
H6A	0.113	0.039	0.149	0.095
C1A	0.057	0.000	-0.278	0.112
Br1B	0.000	-0.087	0.281	-0.171
N1B	-0.287	-0.199	-0.035	-0.087
N2B	-0.107	-0.127	-0.110	-0.155
C2B	-0.166	-0.060	-0.127	-0.219
H2B	0.117	0.030	0.144	0.094
C3B	-0.100	-0.054	-0.160	-0.193
H3B	0.112	0.045	0.150	0.134
C4B	-0.103	-0.019	-0.385	0.176
C5B	-0.106	-0.057	-0.162	-0.175
H5B	0.113	0.045	0.151	0.132
C6B	-0.143	-0.056	-0.118	-0.238
H6B	0.113	0.039	0.149	0.095
C1B	0.057	0.000	-0.278	0.114
Total	-1.000	-1.000	-1.000	-1.000

2.6 Molecular Orbital Diagram

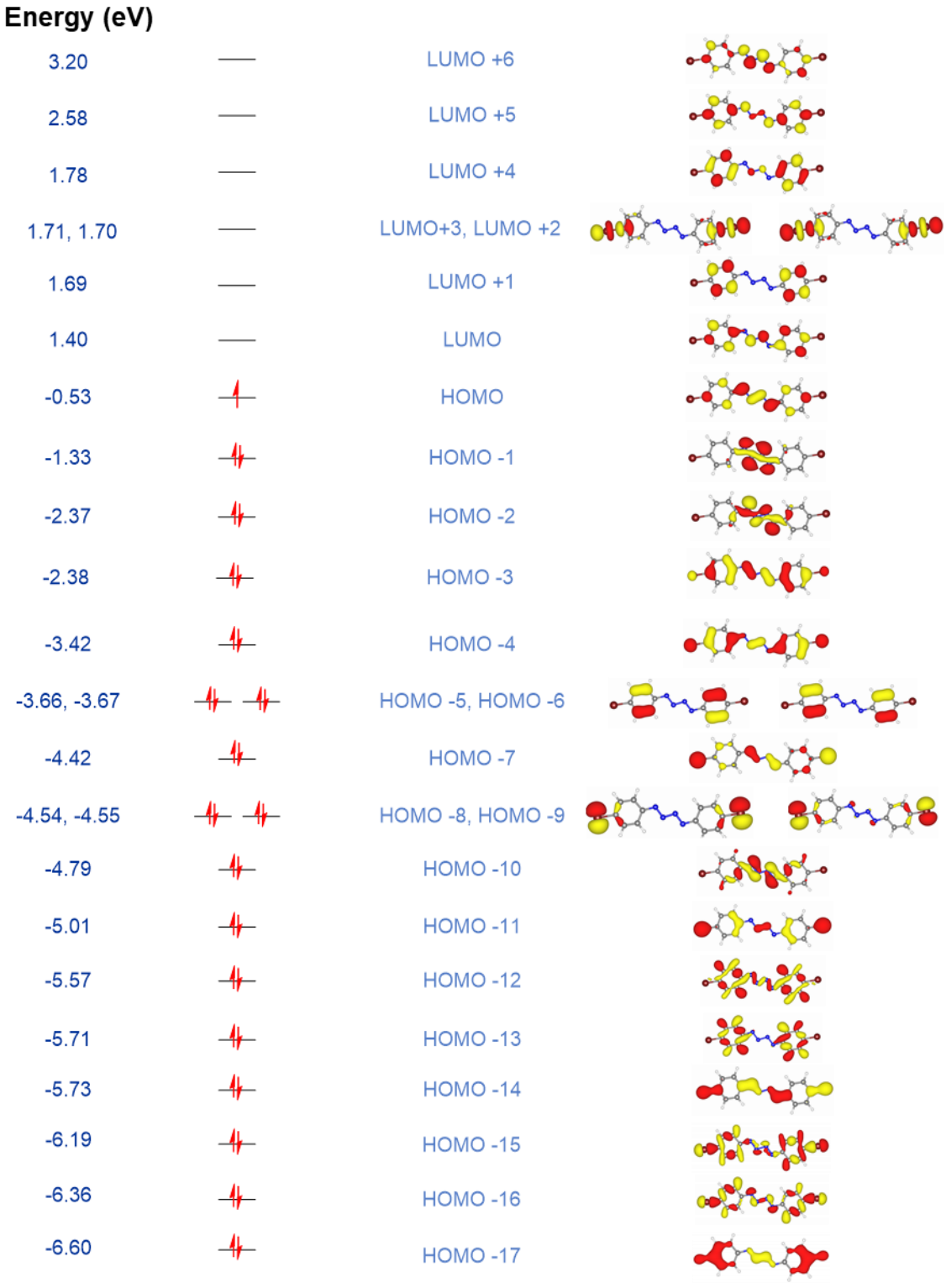

Figure S4: Molecular orbital diagram of [**1**]$^{\bullet-}$ from HOMO-17 to LUMO+6.

2.7 EPR of [K(crypt)][1]

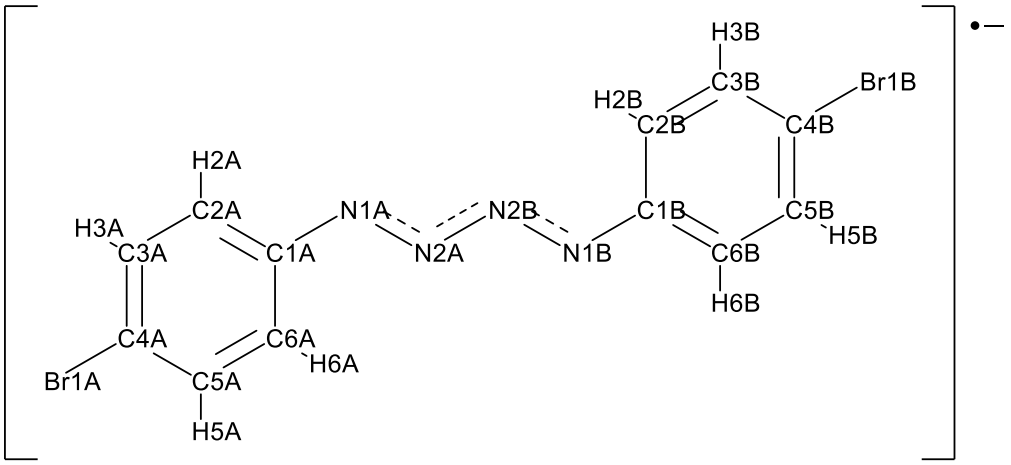

2.7.1 EPR of [K(crypt)][**1**] stacked with a simulation of [**1**]$^{\bullet-}$ using calculated hyperfine values.

Table S5: Calculated A_{iso} values using at B3LYP/EPR-III (aug-cc-PVTZ for Br)/THF.

Atom	A_{iso}	Atom	A_{iso}
N1A	13.0996	N1B	13.1001
N2A	0.0948	N2B	0.0953
H2A	7.0883	H2B	7.0882
H3A	3.2410	H3B	3.2407
H5A	3.3310	H5B	3.3308
H6A	8.2026	H6B	8.2018
Br1A	1.4442	Br1B	1.4444

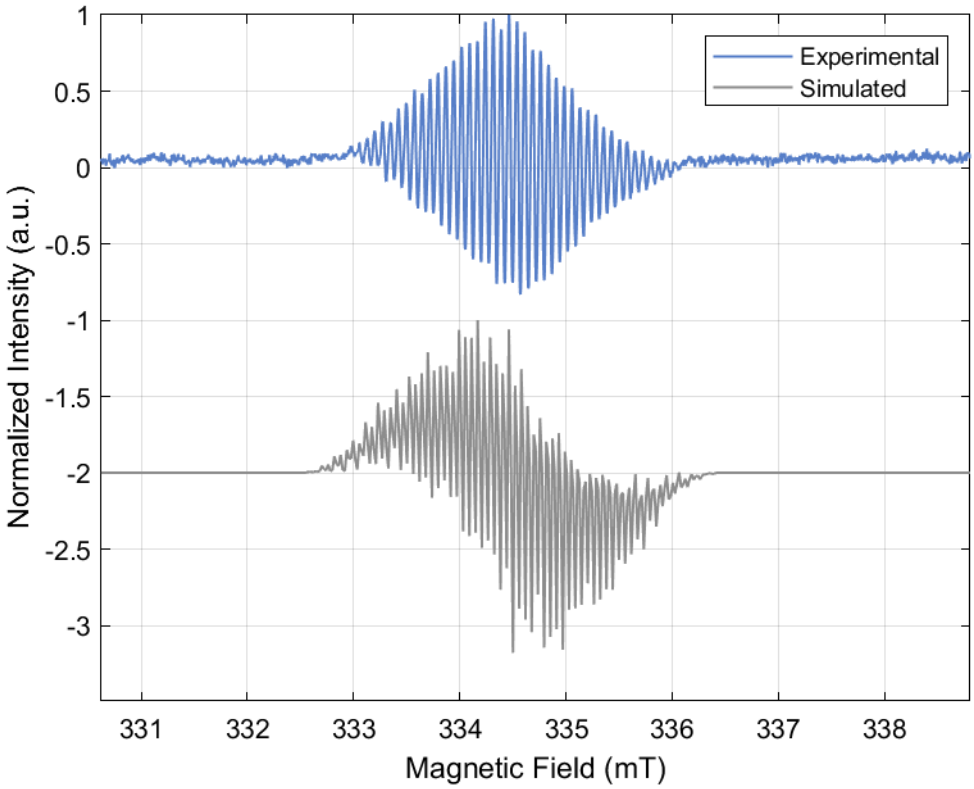

Figure S5: Continuous wave EPR spectrum of [K(crypt)[**1**] stacked above the simulated spectrum of [**1**]$^{\bullet-}$ using the above calculated hyperfine values from Table S5. Experimental parameters: solvent: THF, frequency: 9.389934 GHz, temperature: 298 K, modulation amplitude: 0.100 G, scans: 2, gain: 30 dB.

2.7.2 EPR of [K(crypt)][**1**] stacked with a simplified simulation

A simplified simulation containing only three nuclei environments was attempted to elucidate the key electron – nuclei hyperfine couplings seen in the spectra. These were determined to be two nitrogens with A_N = 14.50 MHz, four hydrogens with A_H = 4.20 MHz and four hydrogens with A_H = 1.92 MHz. These parameters closely reproduce the experimentally measured spectra indicating that these are the most important interactions (See Figure S6 and Figure S7).

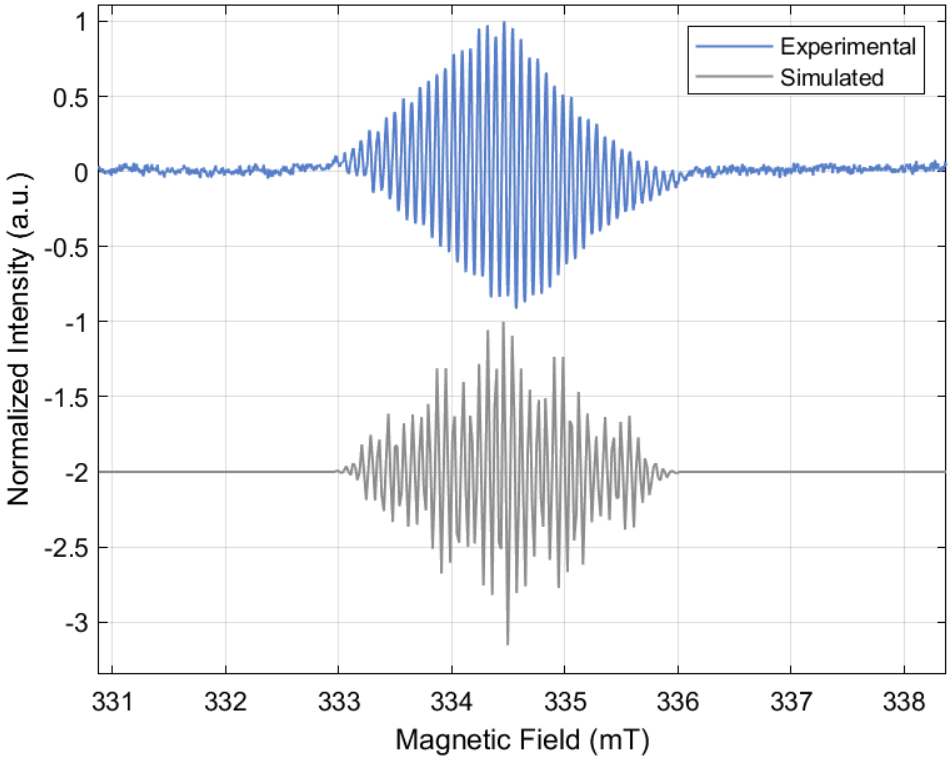

Figure S6: Continuous wave EPR of [K(crypt)][**1**] (blue) stacked above the simulated spectra (grey, ×2 A_N = 14.5 MHz, ×4 A_H = 4.20 MHz, ×4 A_H = 1.92 MHz, g = 200575, lw = 0.04). Experimental parameters: solvent: THF, frequency: 9.389934 GHz, temperature: 298 K, modulation amplitude: 0.100 G, scans: 2, gain: 30 dB.

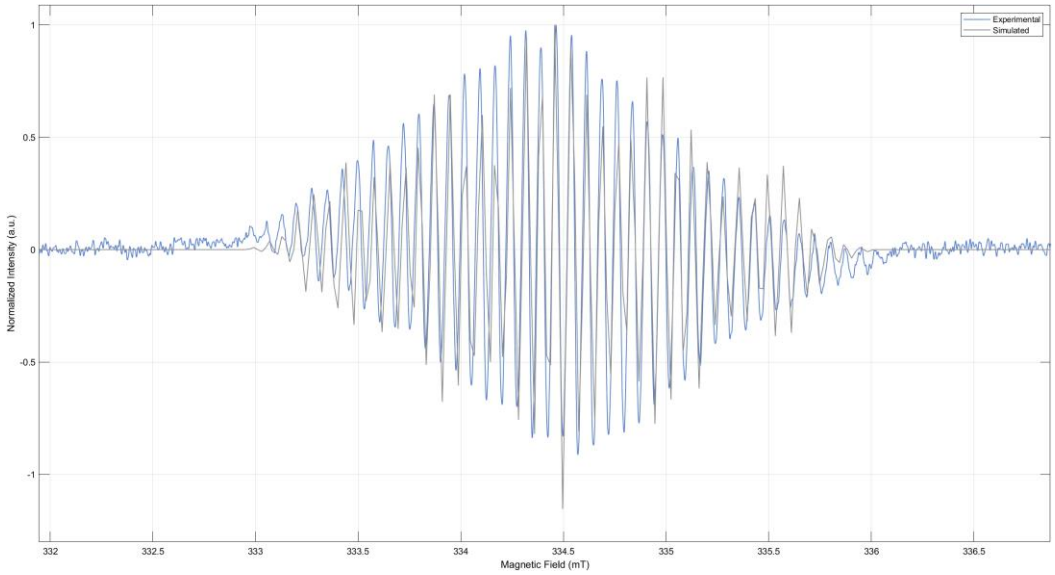

Figure S7: Continuous wave EPR of [K(crypt)][**1**] (blue) overlayed with the simulated spectra (grey, ×2 A_N = 14.5 MHz, ×4 A_H = 4.20 MHz, ×4 A_H = 1.92 MHz, g = 200575, lw = 0.04). Experimental parameters: solvent: THF, frequency: 9.389934 GHz, temperature: 298 K, modulation amplitude: 0.100 G, scans: 2, gain: 30 dB.

2.8 Calculated Spin Densities of $[1]^{\bullet-}$

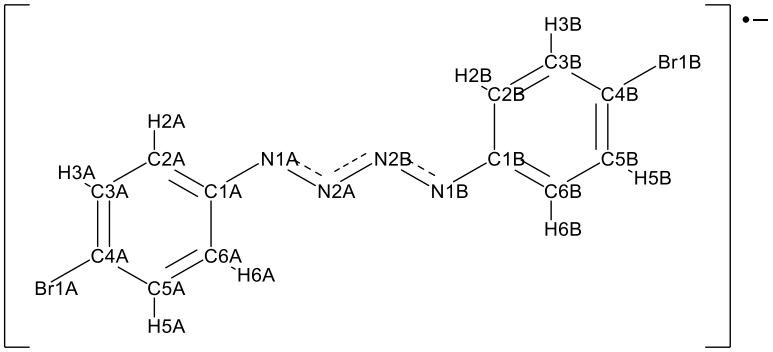

Table S6: Calculated Hirshfeld, Löwdin, and Mulliken spin densities for [**1**]$^{\bullet-}$

Atom	**Spin Number**		
	Hirshfeld	**Löwdin**	**Mulliken**
Br1A	0.018	0.016	0.009
N1A	0.226	0.228	0.263
N2A	0.066	0.063	0.049
C2A	0.067	0.068	0.114
H2A	0.005	0.000	-0.007
C3A	-0.011	-0.009	-0.047
H3A	-0.001	0.000	0.002
C4A	0.075	0.074	0.113
C5A	-0.010	-0.008	-0.042
H5A	-0.001	0.000	0.002
C6A	0.058	0.056	0.091
H6A	0.003	0.000	-0.004
C1A	0.005	0.011	-0.040
Br1B	0.018	0.016	0.009
N1B	0.226	0.228	0.262
N2B	0.066	0.063	0.048
C2B	0.067	0.068	0.111
H2B	0.005	0.000	-0.006
C3B	-0.011	-0.009	-0.046
H3B	-0.001	0.000	0.002
C4B	0.075	0.074	0.111
C5B	-0.010	-0.008	-0.042
H5B	-0.001	0.000	0.002
C6B	0.058	0.056	0.090
H6B	0.003	0.000	-0.004
C1B	0.005	0.011	-0.040
Total	1.000	1.000	1.000

2.9 Spin Counting of [K(crypt)][1]

To further confirm purity, a spin counting experiment was done.

3.7mg of [K(crypt)][**1**] was dissolved in 2 mL 50:50 mixture of *o*DFB : toluene. A 0.5 mL aliquot was taken and diluted with 1.5 mL of 50:50 *o*DFB : toluene to make a 0.59 mM sample. 0.3 mL was added to a J Young EPR tube in order to fill the whole resonator and immediately frozen in liquid nitrogen until it was ready to be measured. A spin number of 3 x 10^{16} was calculated indicating a radical concentration of 0.586 mM using the equation from the calibration curve trendline which was measured using a standard sample of TEMPO diluted to different concentrations. This result shows that there is near complete conversion and retention of the radical form [K(crypt)][**1**].

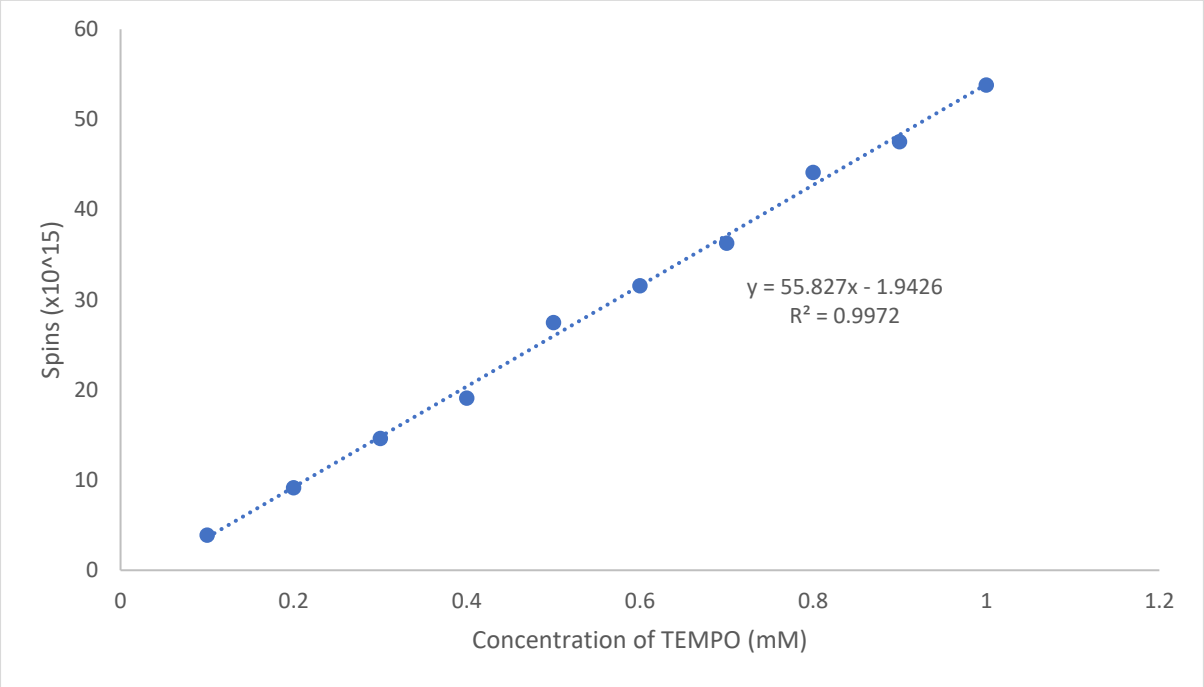

Figure S8: Calibration curve for spin counting with a varying TEMPO concentration; equation of the straight line used to calculate spins in [K(crypt)][**1**] is shown.

2.10 Assessing Stability of [K(crypt)][1]

To assess the effect of solvents on the half-life of [K(crypt)][**1**], a 2D continuous wave EPR technique was used where a spectrum is collected in consistent intervals and the max peak intensity of spectra can be tracked over time and plotted as a decay curve.

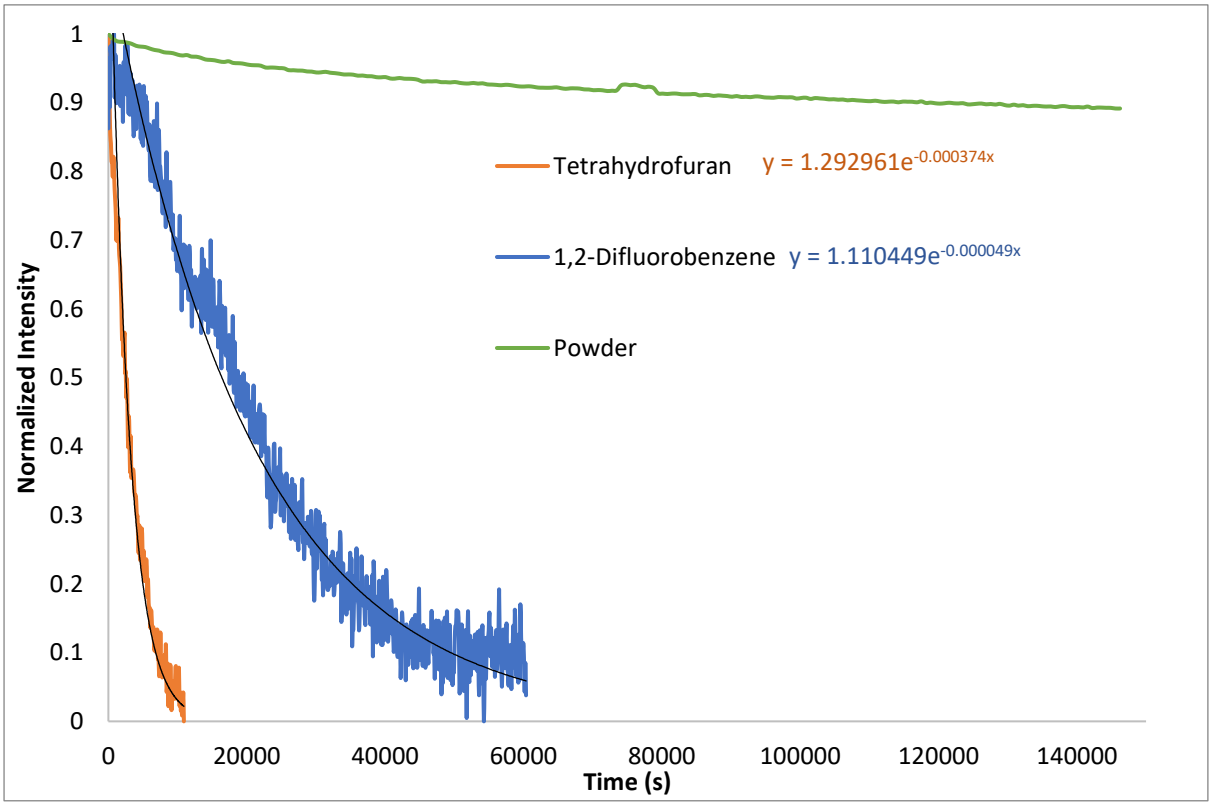

Figure S9: Decay curve of [K(crypt)][**1**] in THF (orange), *o*DFB (blue) and powder (green) with the exponential equation shown beside the legend.

Table S7: Calculated half-life's of [K(crypt)][**1**] in THF and *o*DFB using exponential decay curve equation.

Solvent	**Half-life (s)**
THF	1853 (30.8 mins)
*o*DFB	14146 (235.8 mins)

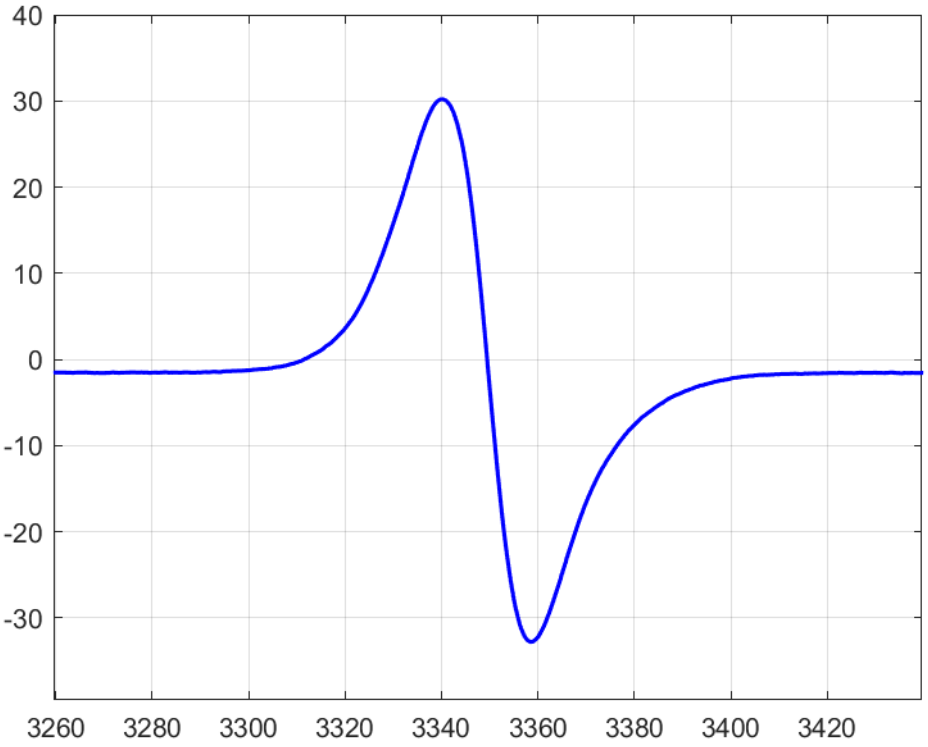

Figure S10: Continuous wave EPR spectra (solid state) of [K(crypt)][**1**] after 6 weeks under inert atmosphere at room temperature.

2.11 SQUID Measurements of [K(crypt)][1]

Squid measurements were completed on a ground up crystalline sample of [K(crypt)][**1**] in a gelatine capsule. Diamagnetic contributions of the capsule were accounted for using data from a blank gelatine capsule and the diamagnetic contribution of the molecule was estimated according to literature procedure.[27]

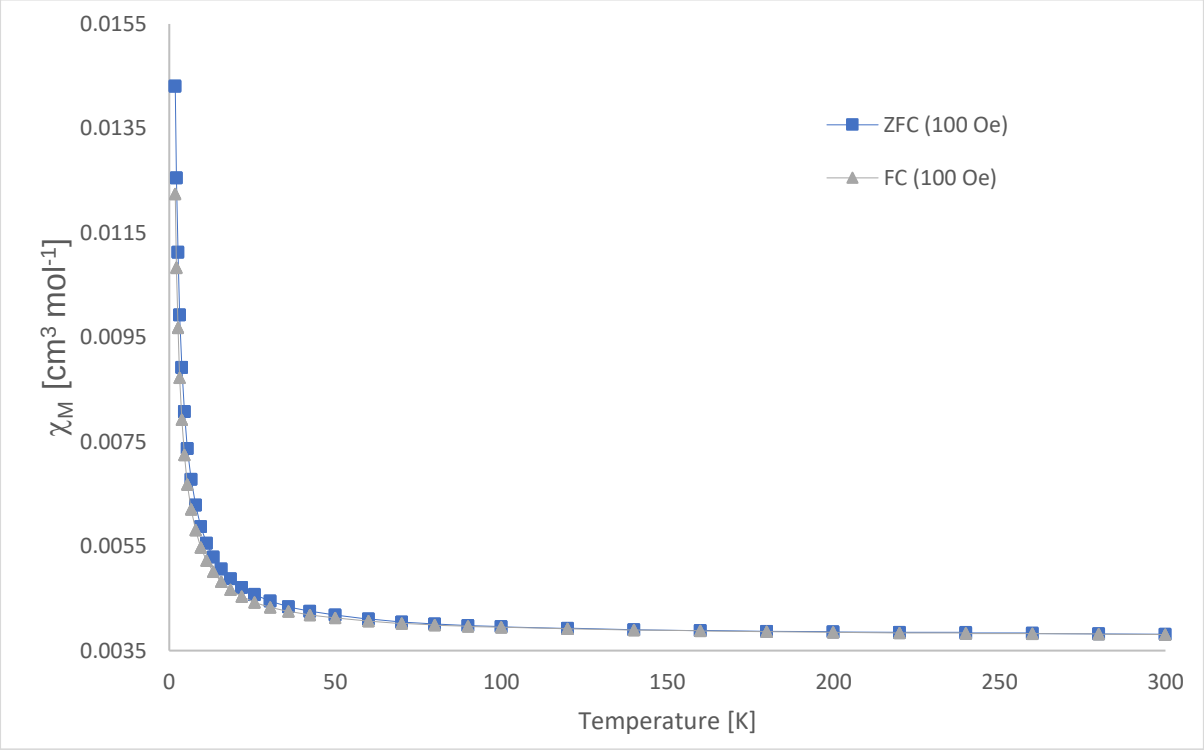

Figure S11: Molar magnetic susceptibility, χ_M, of [K(crypt)][**1**]. Blue squares refer to zero field cooled and grey triangle refer to field cooled recordings of magnetic susceptibility at 100 Oe.

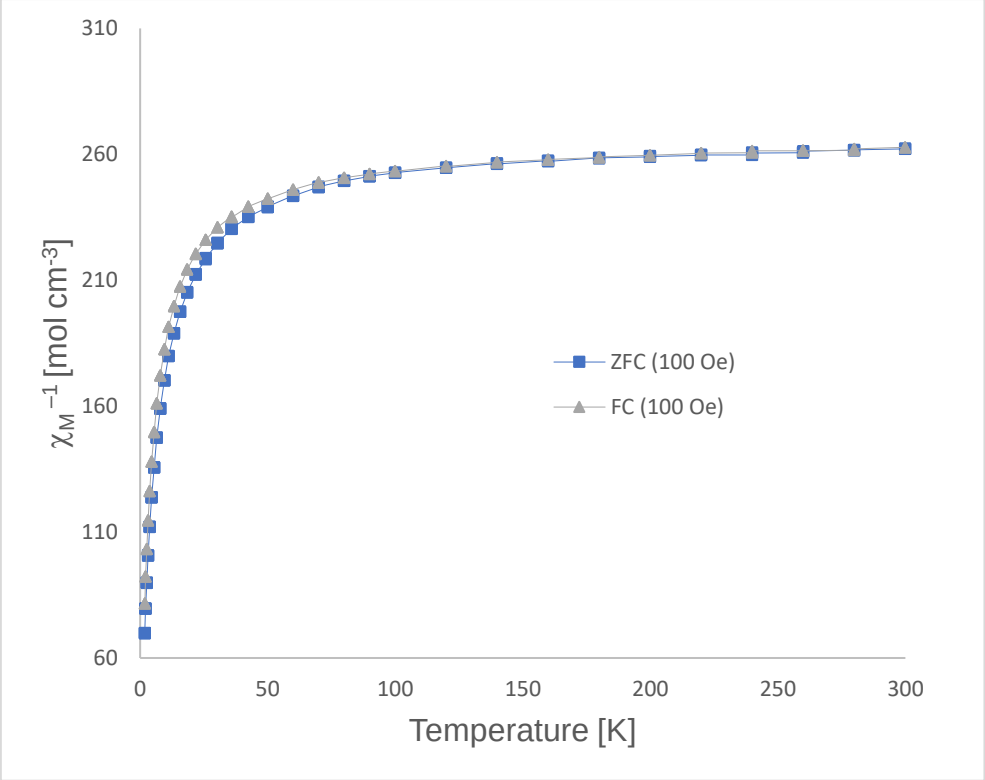

Figure S12: Inverse of molar magnetic susceptibility, χ_M^{-1}, of [K(crypt)][**1**]. Blue squares refer to zero field cooled and grey triangle refer to field cooled recordings of magnetic susceptibility at 100 Oe.

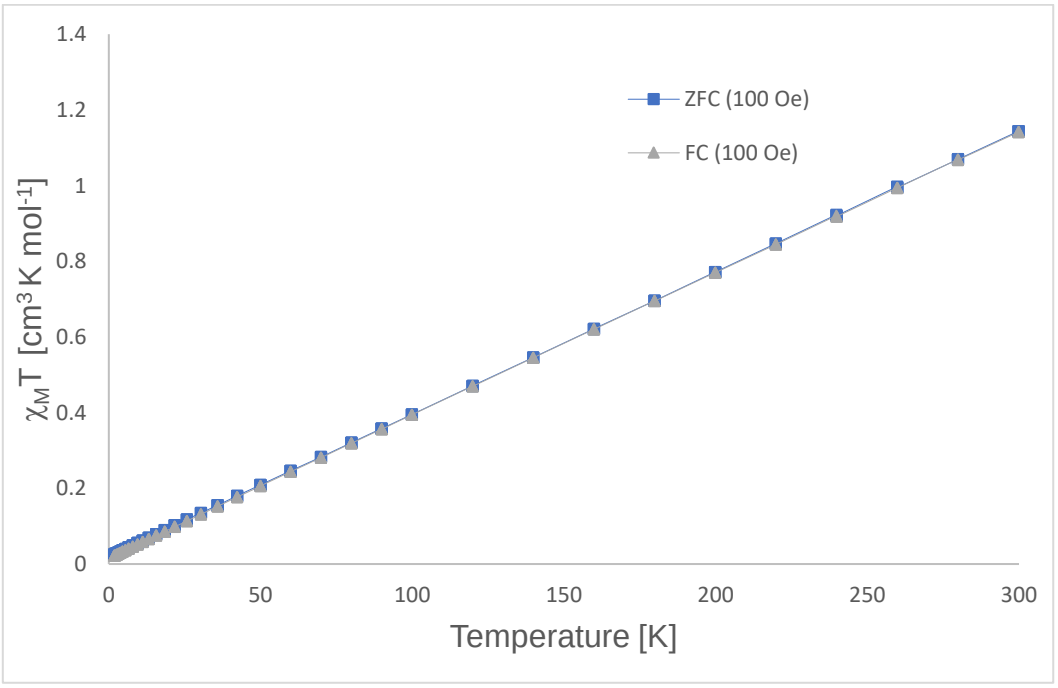

Figure S13: $\chi_M T$ of [K(crypt)][**1**] vs temperature. Blue squares refer to zero field cooled and grey triangle refer to field cooled recordings of magnetic susceptibility at 100 Oe.

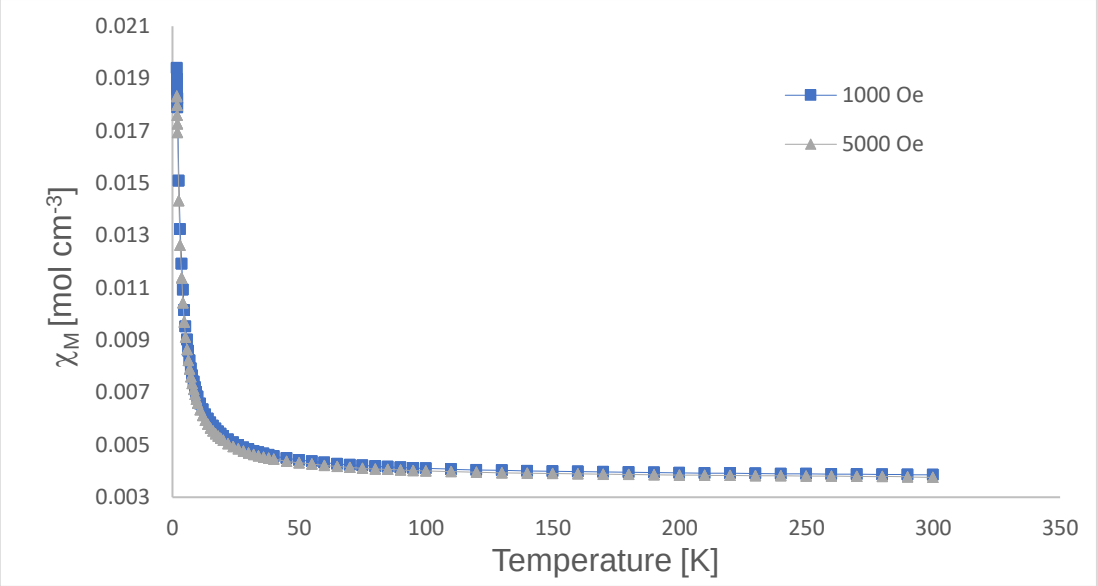

Figure S14: Molar magnetic susceptibility, χ_M, of [K(crypt)][**1**]. Blue squares refer a field strength of 1000 Oe and grey triangles refer to a field strength of 5000 Oe.

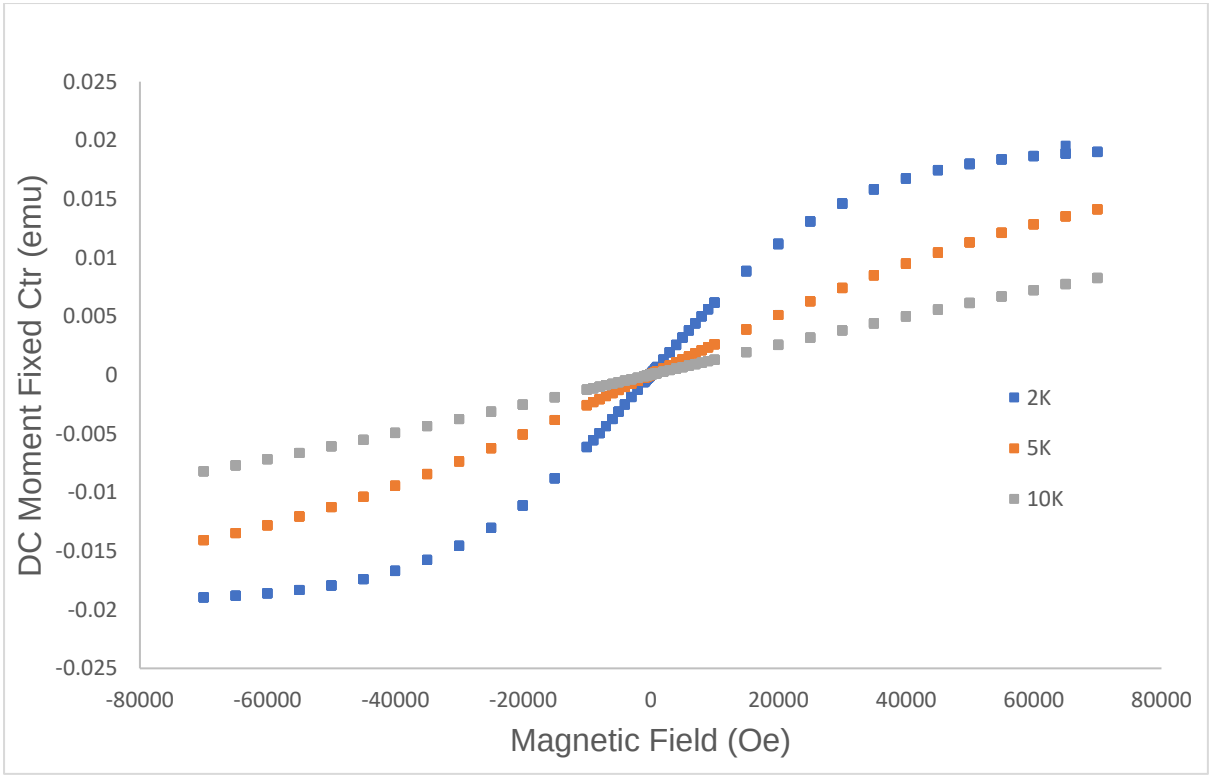

Figure S15: A graph of magnetization v applied field at varying temperatures. Blue squares refer to a temperature of 2 K, orange squares refer to 5 K and grey squares refer to 10 K.

2.12 Cyclic Voltammetry of [K(crypt)][1]

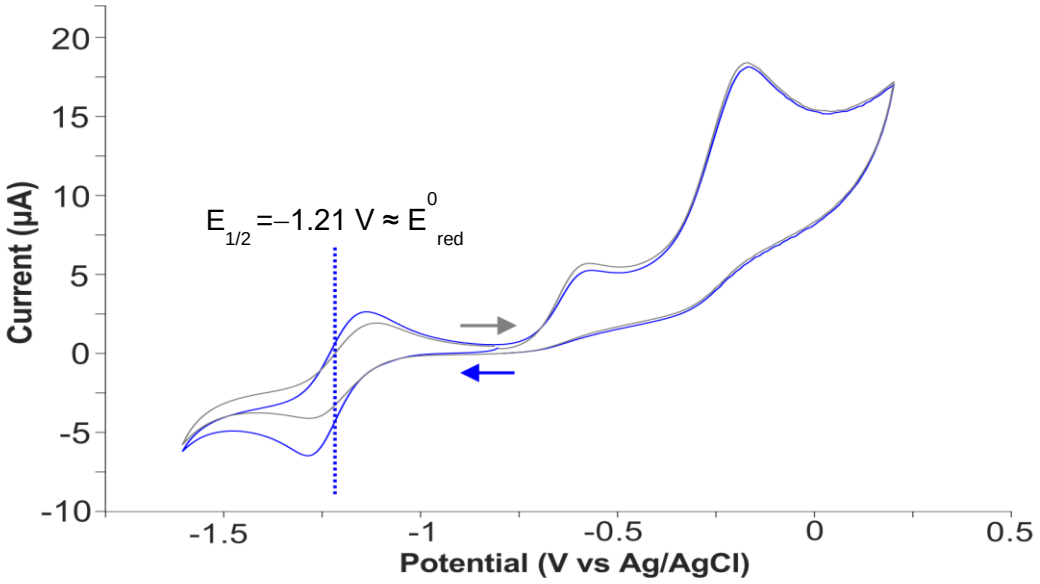

Figure S16: Cyclic Voltammetry of [K(crypt)][**1**] 3 mM in THF with [nBu_4N][PF_6] electrolyte at 0.1 V/s starting at –0.8 V and scanning independently in the positive direction first (grey trace) and the negative direction first (blue trace). Glassy carbon working electrode, platinum wire counter electrode and leak-proof Ag/AgCl reference electrode were used.

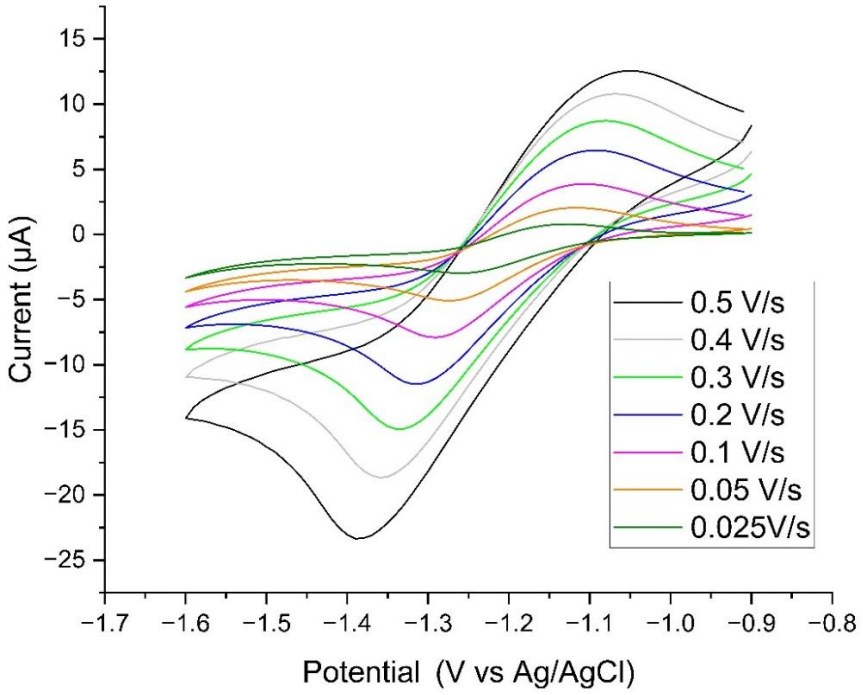

Figure S17: Cyclic Voltammetry of [K(crypt)][**1**] 0.3 M in THF with [nBu_4N][PF_6] electrolyte at varying scan rates on first reduction wave using glassy carbon working electrode, platinum wire counter electrode and leak-proof Ag/AgCl reference electrode.

2.13 Infrared Spectroscopy of [K(crypt)][1]

When comparing the IR of [K(crypt)][**1**] to [K(crypt)][Cl] (Figure S20, zoomed in), we can see a major new peak at 1236 cm^{-1} which is between the stretching frequencies of hydrazine (1077 cm^{-1}) and azobenzene (1439 cm^{-1}).[28, 29] This is believed to be associated with N–N bond stretches, and is in good agreement with the calculated IR stretches (1272 cm^{-1}) (Figure S21 and S22).

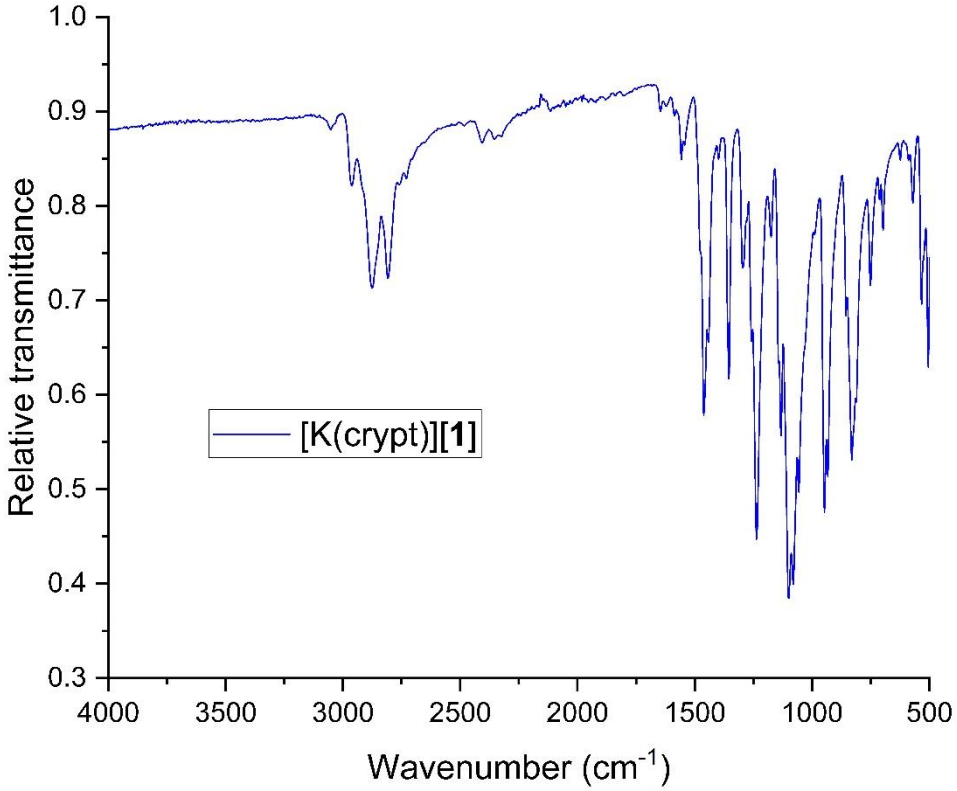

Figure S18: Full solid state IR spectrum of [K(crypt)][**1**]

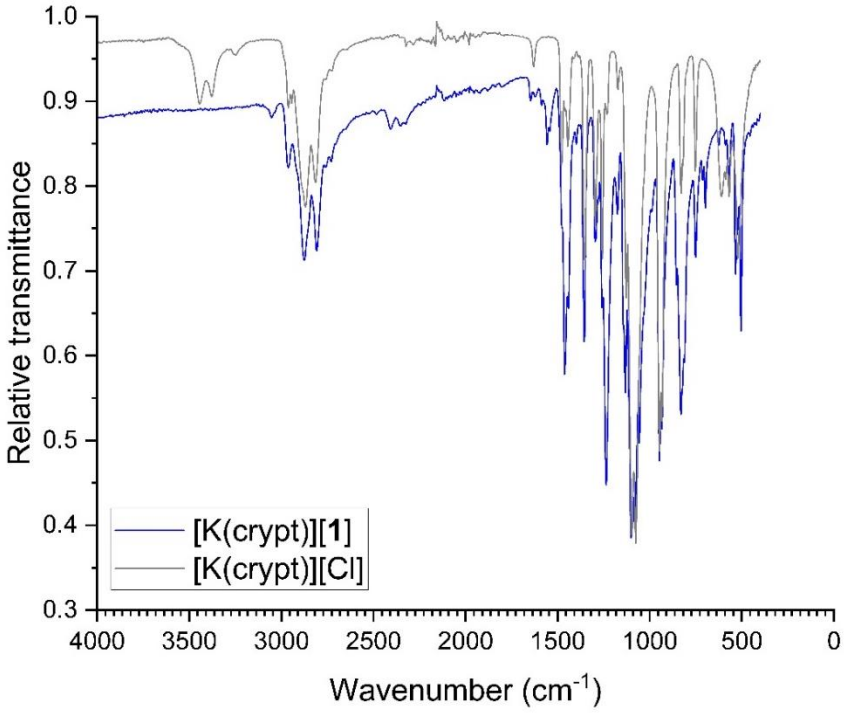

Figure S19: Solid state IR spectrum of [K(crypt)][**1**] overlayed with independently prepared [K(crypt)][Cl].

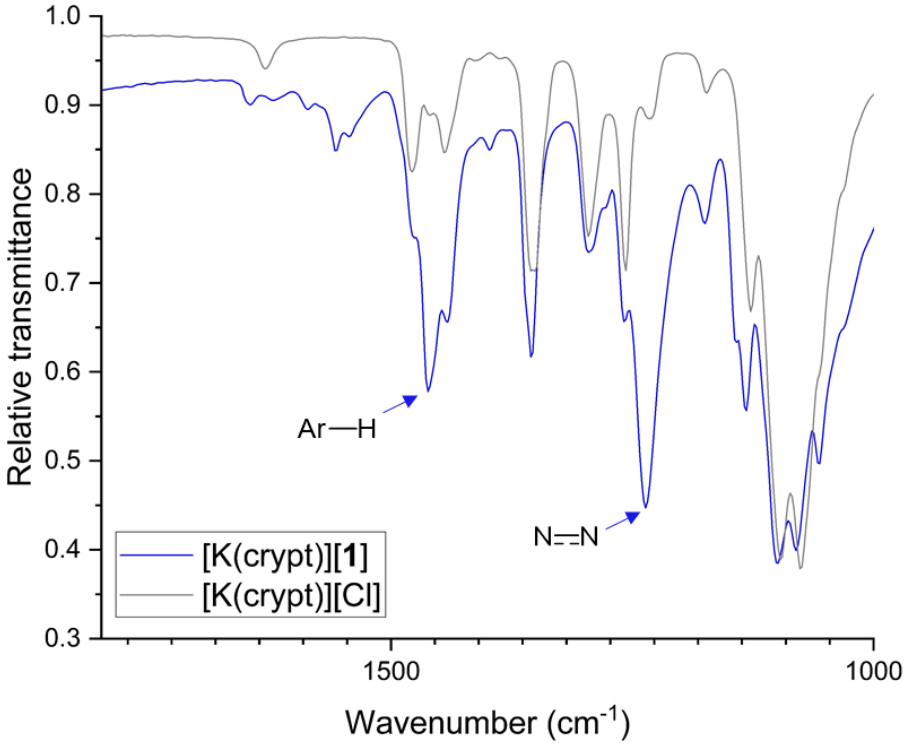

Figure S20: Zoomed in solid state IR spectrum of [K(crypt)][**1**] overlayed with independently prepared [K(crypt)][Cl] with key peaks from [**1**]$^{\bullet-}$ highlighted.

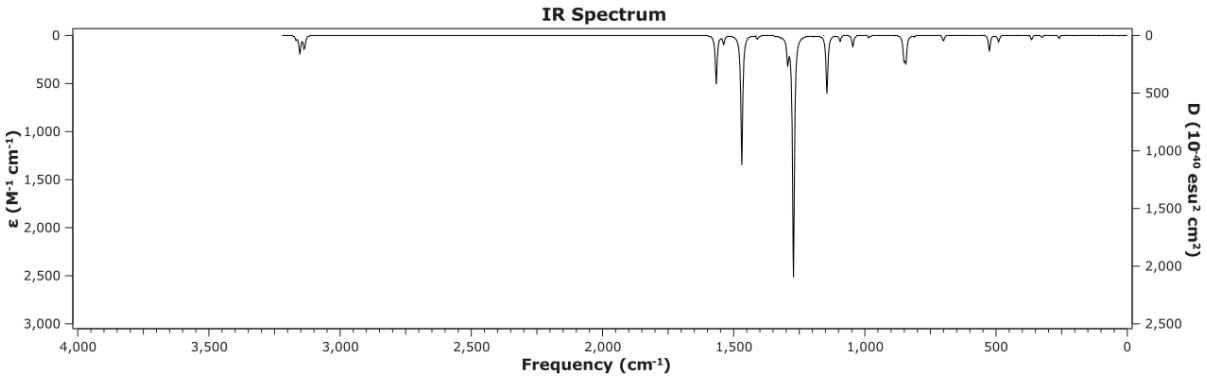

Figure S21: Calculated IR spectrum of [**1**]$^{\bullet-}$.

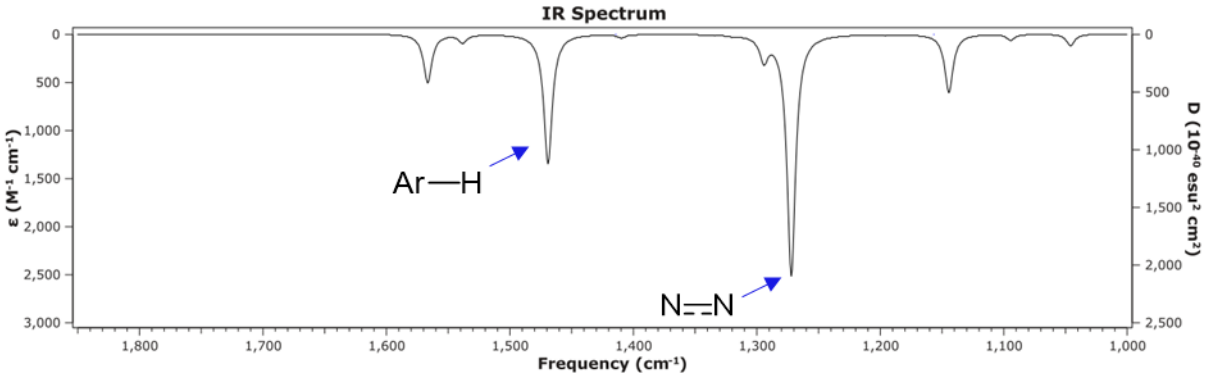

Figure S22: Zoomed in calculated IR spectrum of [**1**]$^{\bullet-}$ with key peaks highlighted.

2.14 Ultraviolet-visible Spectroscopy of [K(crypt)][1]

2.14.1 Observed UV-vis of [K(crypt)][**1**]

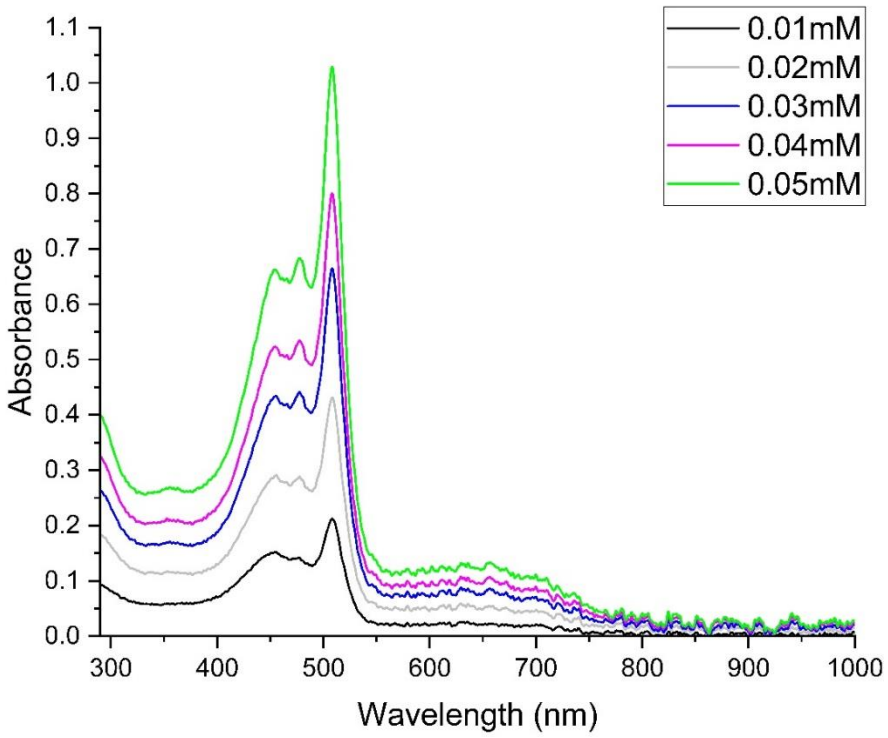

Figure S23: UV-Vis spectra of [K(crypt)][**1**] at a range of concentrations from 0.01 mM to 0.05 mM in *o*DFB.

2.14.2 Calculated UV-Vis Transitions

To characterise the UV/Vis absorption spectra of [**1**]$^{\bullet-}$, TD-DFT calculations were performed on the geometry previously optimized at Def2-TZVP/TPSS, using a variety of functionals (Table S8 below). The key transitions found experimentally at 355 nm, 454 nm, 508 nm and 612 nm were best reproduced by the TPSSh functional. The orbital make-up of the transitions is complicated at the Kohn-Sham level, so to better understand the origin of the computed transitions, the Natural Transition Orbitals (NTOs) associated with each transition were calculated, revealing that all four of the excited states were underpinned by transitions 90α → 91α (grey dot) and 89β → 90β (blue dot), with different occupations (Figure S24).

Table S8: Experimental and calculated UV wavelengths and oscillator strengths for transitions to selected excited states for [**1**]$^{\bullet-}$ for a variety of functionals and solvents (experimental absorbance is compared with computed oscillator strength).

Method/ Solvent	**Excited State 1**		**Excited State 2**		**Excited State 3**		**Excited State 4**	
	Wavelength (nm)	**Oscillator Strength**	**Wavelength (nm)**	**Oscillator Strength**	**Wavelength (nm)**	**Oscillator Strength**	**Wavelength (nm)**	**Oscillator Strength**
Experimental/*o*DFB	~355	~0.27	~454	~0.66	~508	~1.03	~612	~0.13
PBE/THF	378.66	0.019	487.62	1.25	538.76	0.316	663.19	0.001
PBE0/THF	314.45	0.017	406.30	0.195	474.87	1.379	579.45	0.034
TPSS/THF	366.43	0.023	473.70	1.05	515.92	0.538	645.59	0.004
TPSSh/THF	337.60	0.049	441.72	0.437	487.76	1.167	612.00	0.013
B3LYP/THF	329.14	0.067	423.99	0.250	484.42	1.320	598.67	0.013
CAM-B3LYP/THF[30]	282.68	0.011	360.88	0.112	466.01	1.357	540.96	0.072
B3PW91/THF[19]	328.16	0.063	421.27	0.249	480.28	1.338	593.67	0.019
M06-2X/THF[31]	299.75	0.068	363.24	0.122	453.07	1.481	527.85	0.003
ωB97XD/THF	278.78	0.020	355.24	0.100	460.52	1.399	533.90	0.057
TPSS/cyclopentanone	369.58	0.025	472.16	0.892	513.84	0.693	646.76	0.007
TPSSh/cyclopentanone	339.86	0.049	437.56	0.358	488.29	1.237	612.89	0.017
B3LYP/cyclopentanone	329.98	0.074	419.47	0.217	485.66	1.343	599.64	0.017

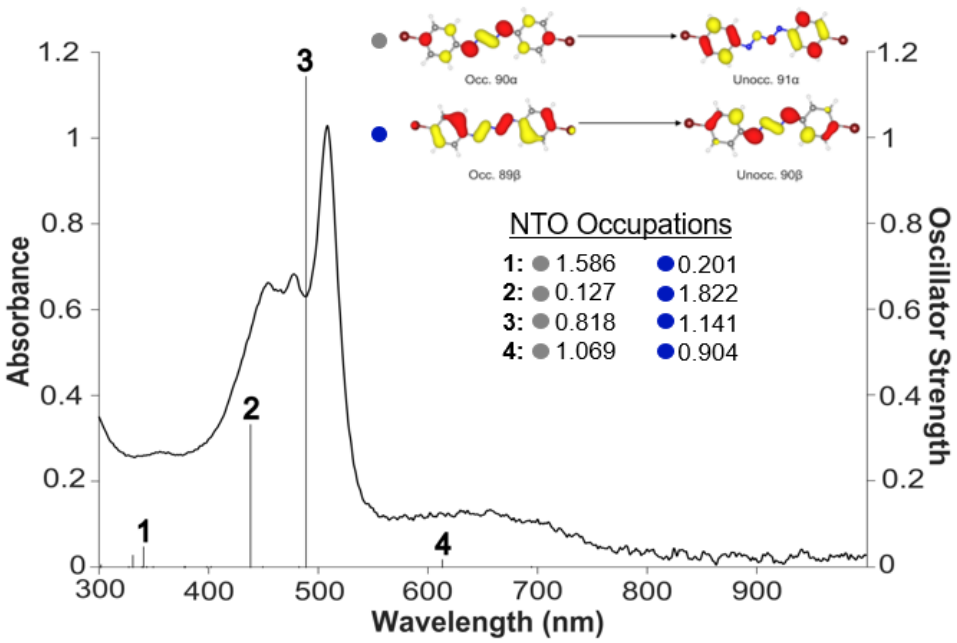

Figure S24: Calculated UV-Vis spectrum of [**1**]$^{\bullet-}$, showing the key natural transition orbitals (NTOs) and their occupations with blue and grey dots in computed transitions 1–4.

3. Reactivity Studies

3.1 Isolation of $[2]^{2-}$

In a vial in the glovebox, 4-$BrC_6H_4N_3$ (29.5 mg, 0.235 mmol, 1 equiv.) and KC_8 (31.5 mg, 0.235 mmol, 1 equiv.) were suspended in THF resulting in a red solution. The reaction mixture was filtered and hexane added to the filtrate yielding a red solid. Recrystallization from vapour diffusion of hexane into a THF solution at –40 °C yielded crystals of $[K(THF)_2]_2$[**2**] suitable for XRD studies.

Author's Note: The crystal data unambiguously shows the presence of $[K(THF)_2]_2$[**2**] with an occupancy of 60%. Evidence of a secondary species is present but this species can not be fully identified, at this stage we speculate that this secondary species may be 4-$BrC_6H_4N_2^-$. Further characterization could not be obtained as $[K(THF)_2]_2$[**2**] detonates when shocked under an inert atmosphere or when exposed to air.

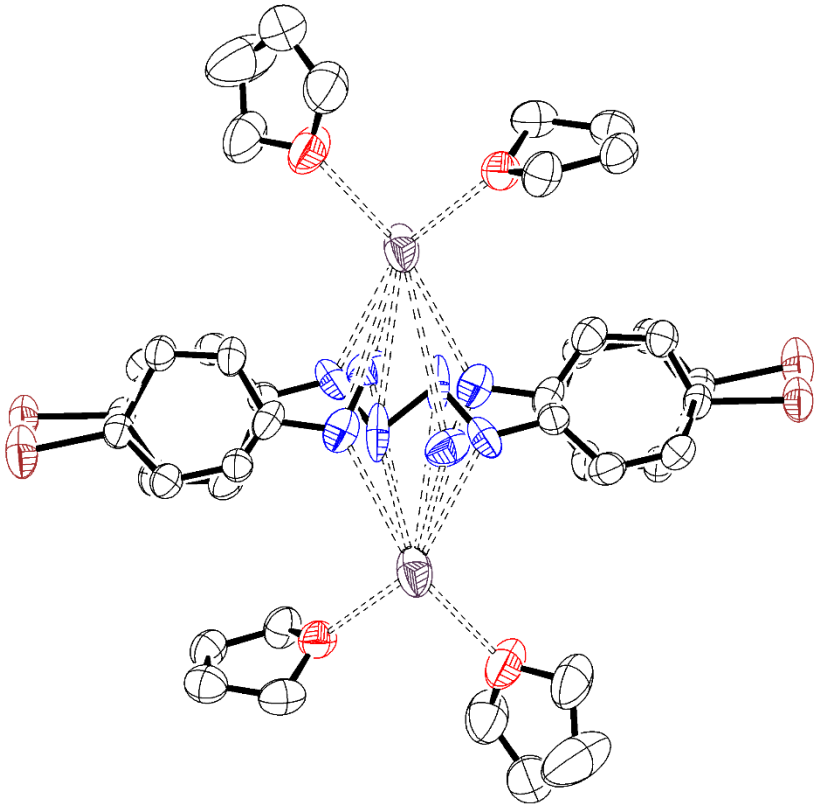

Figure S25: Molecular structure of $[K(THF)_2]_2$[**2**] showing anisotropic displacement ellipsoids at 50% probability with hydrogen atoms omitted for clarity. Nitrogen: blue; carbon: white; bromine: brown; potassium: violet; oxygen: red.

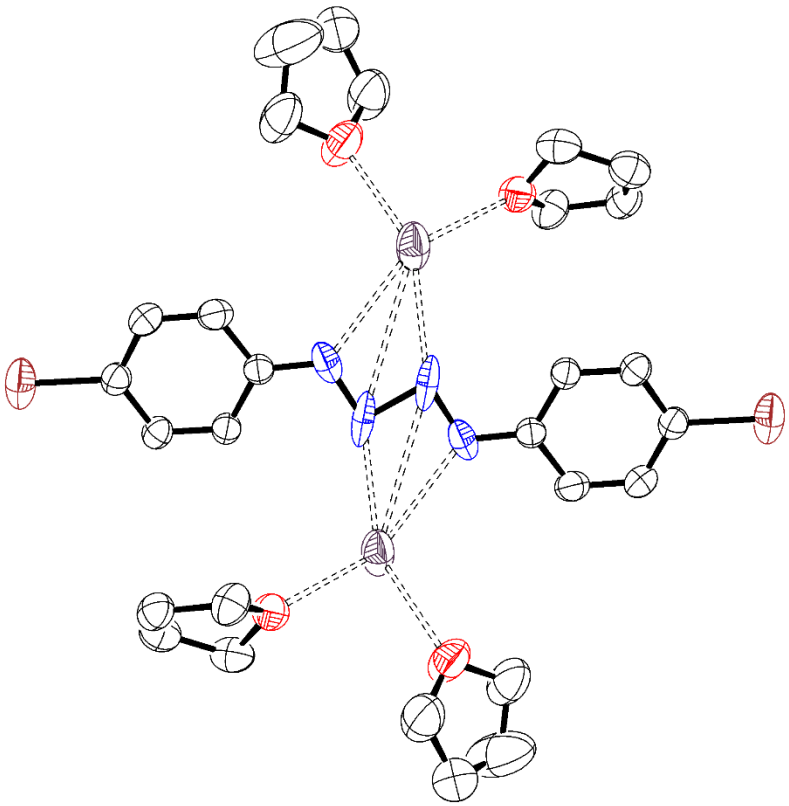

Figure S26: Molecular structure of $[K(THF)_2]_2$[**2**] showing anisotropic displacement ellipsoids at 50% probability with hydrogen atoms omitted for clarity. Disorder omitted for clarity and major component (*ca.* 60% occupancy) shown. Nitrogen: blue; carbon: white; bromine: brown; potassium: violet; oxygen: red.

3.2 Addition of Ph_3SnH to [K(crypt)][1]

3.2.1 Addition of Ph_3SnH to [K(crypt)][**1**] with crude NMR

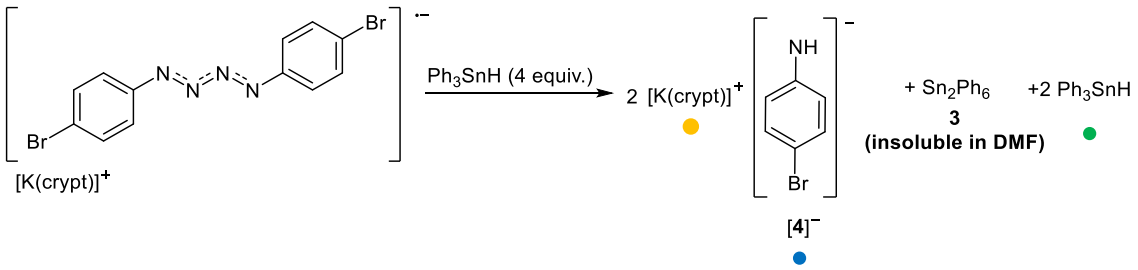

In the glovebox, a solution of Ph_3SnH (12.7 mg, 0.102 mmol, 4 equiv.) in DMF-d_7 (0.5 mL) was added to a vial containing [K(crypt)][**1**] (30.0 mg, 0.039 mmol, 1 equiv.). The solution was shaken for 1 minute before transferring to a J Young NMR tube for analysis by NMR spectroscopy.

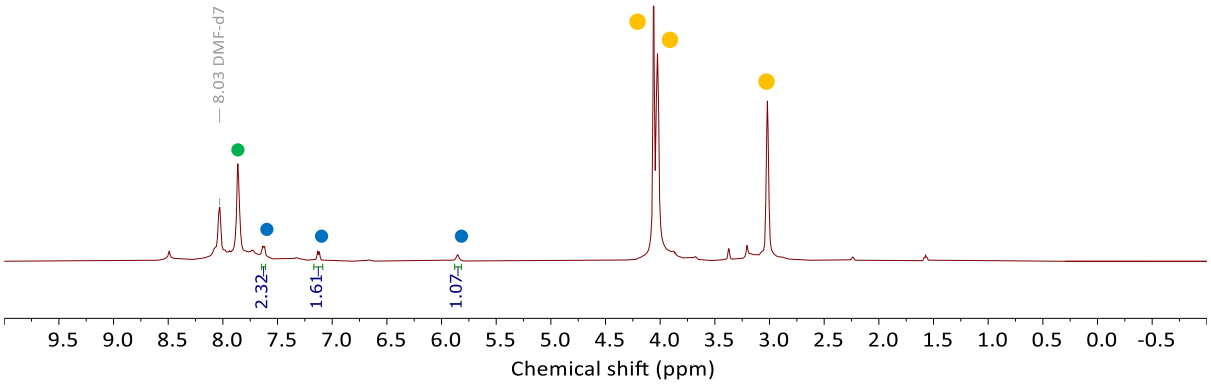

Figure S27: Crude ^1H NMR spectrum (400 MHz, DMF-d_7) of reaction 3.2.1.

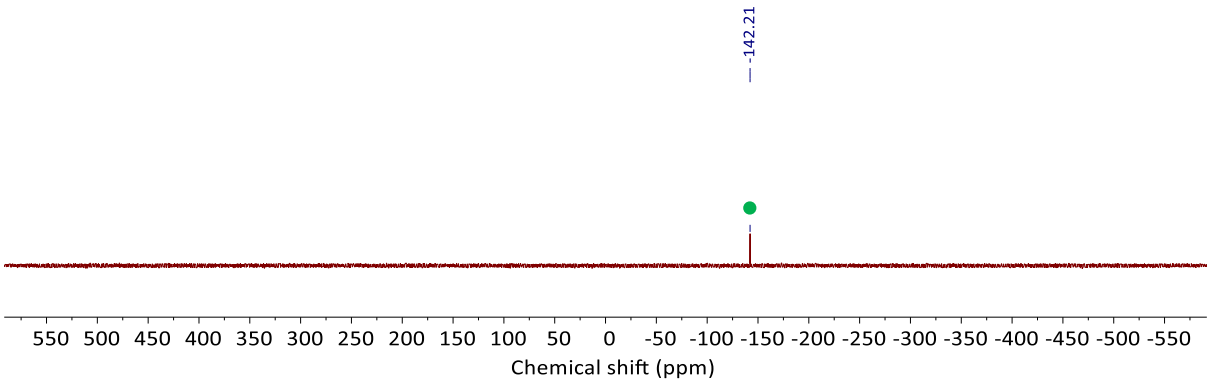

Figure S28: ^{119}Sn NMR spectrum (149 MHz, DMF-d_7) of reaction 3.2.1 showing unreacted Ph_3SnH.

3.2.2 Addition of Ph_3SnH to [K(crypt)][**1**] with aqueous workup

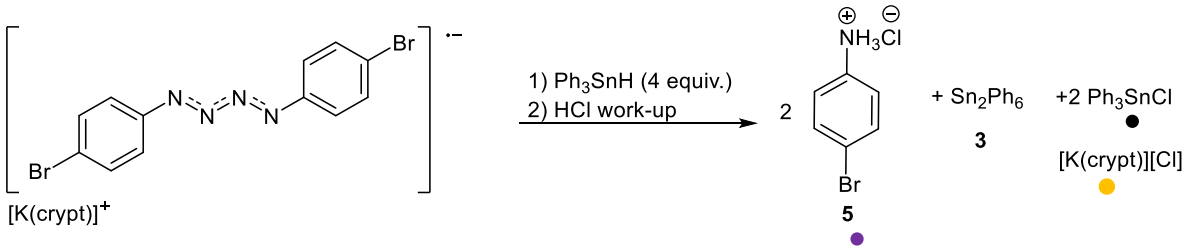

In the glovebox, a solution of Ph_3SnH (12.7 mg, 0.102 mmol, 4 equiv.) in DMF (1 mL) was added to a vial containing [K(crypt)][**1**] (30.0 mg, 0.039 mmol, 1 equiv.). The solution was stirred for 30 minutes yielding Sn_2Ph_6 (**3**) as a white solid which was filtered and recrystallized from benzene.[32] HCl in ether was added to the filtrate and the precipitate filtered and dried yielding 4-bromoanilinium chloride (**5**) which was analyzed by NMR spectroscopy. NMR yields was obtained using Si_2Me_6 (10 µL) as internal standard (^{1}H δ = 0.08 ppm).

NMR conversion of 4-bromophenylammonium chloride (5): 57% (vs Si_2Me_6 internal standard).

Isolated Yield of Sn_2Ph_6: 5.4 mg (85%).

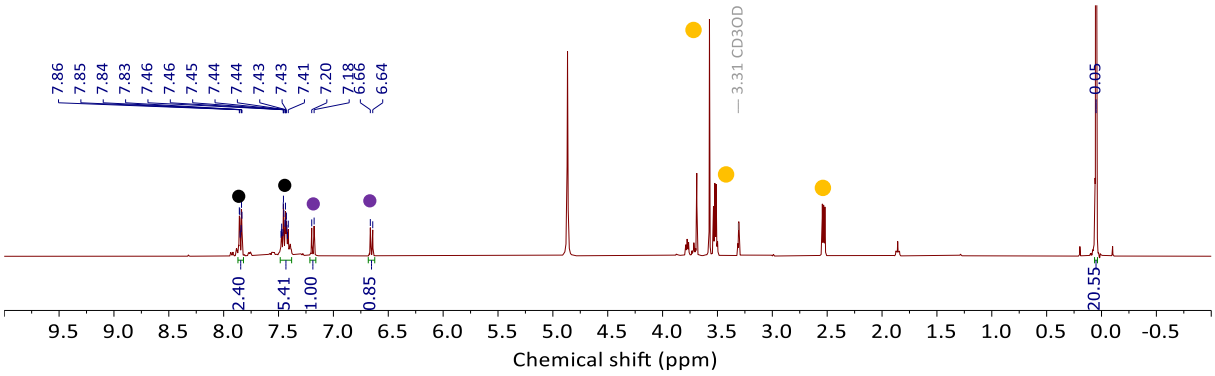

Figure S29: ^{1}H NMR spectrum (400 MHz, MeOD-d_4) of worked up reaction mixture 3.2.2 containing 4-bromoanilinium chloride (**5**). Circles above signals identify the products.

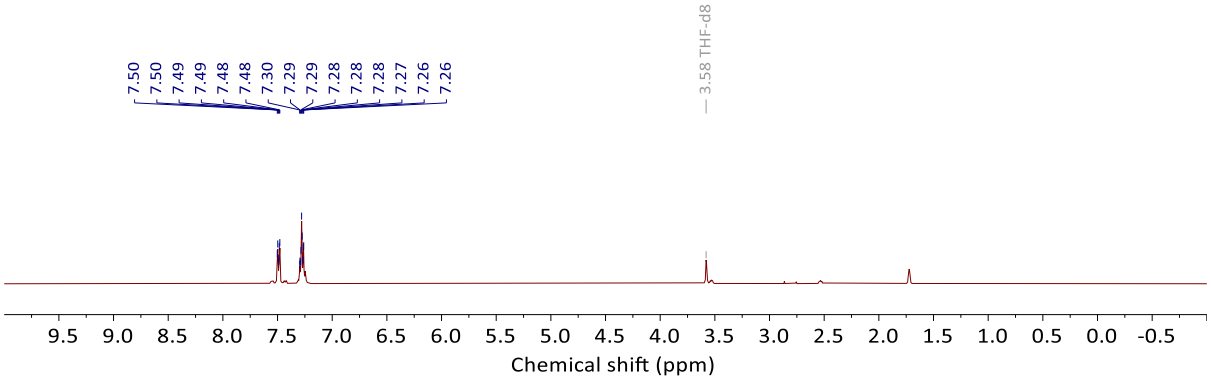

Figure S30: ^{1}H NMR spectrum (400MHz, THF-d_8) of isolated Sn_2Ph_6 (**3**).

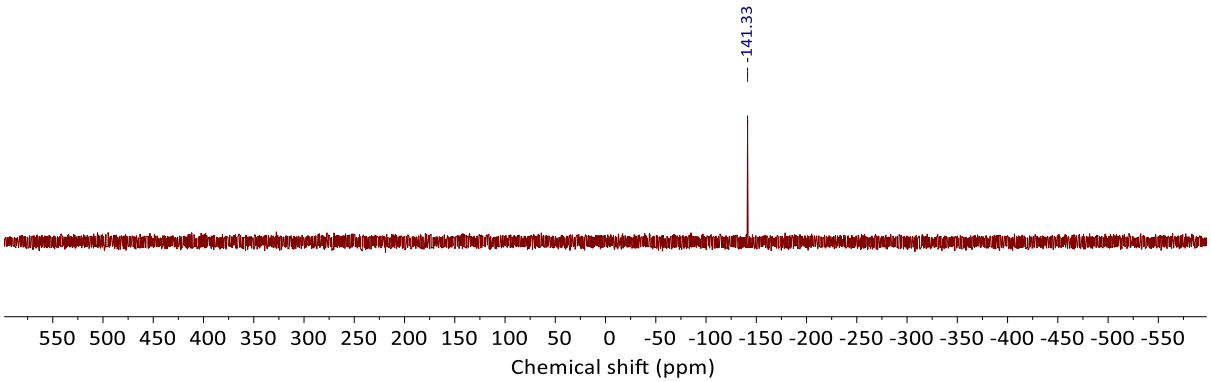

Figure S31: ^{119}Sn NMR spectrum (149 MHz, C_6D_6) of isolated Sn_2Ph_6 (**3**).

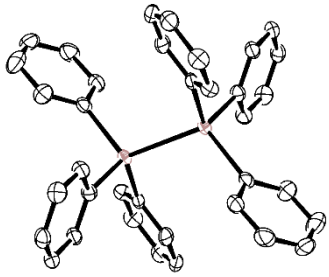

Figure S32: Molecular structure of Sn_2Ph_6 (**3**) obtained from reaction 3.2.2 showing anisotropic displacement ellipsoids at 50% probability with hydrogen atoms omitted for clarity. Tin: pink; carbon: white.

3.3. Addition of TolSH to [K(crypt)][1]

3.3.1. Addition of 1 equivalent of TolSH

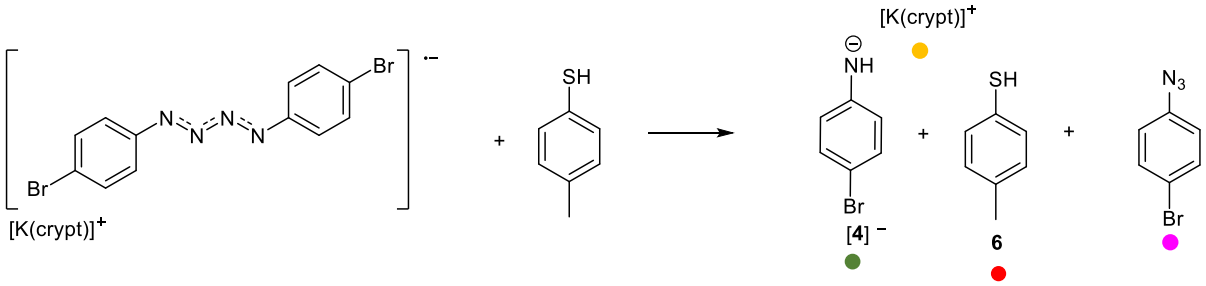

In the glovebox, a solution of TolSH (6.4 mg, 0.026 mmol, 1 equiv.) in THF-d_8 (0.5 mL) was added to a vial containing [K(crypt)][**1**] (20 mg, 0.026 mmol, 1 equiv.). The solution was shaken for 1 minute and filtered into a J Young NMR tube and analyzed by NMR spectroscopy. Single crystals from the reaction were obtained via slow diffusion of hexane into the reaction mixture.

XRD studies confirmed these crystals to be of [K(crypt)][**4**] + **6**. EPR spectroscopy was conducted on the reaction mixture and no resonances were observed, confirming the presence of only diamagnetic products. The presence of 4-$BrC_6H_4N_3$ was confirmed by comparing NMR data from the reaction mixture with that independently acquired for 4-$BrC_6H_4N_3$.

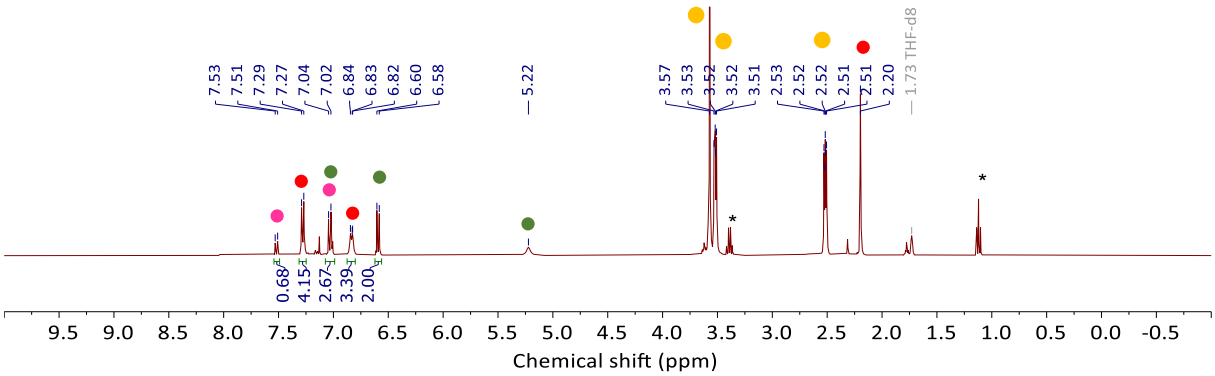

Figure S33: ^{1}H NMR spectrum (400 MHz, THF-d_8) of crude reaction mixture of [K(crypt)][**1**] + TolSH 1:1. Circles above signals identify the products and diethyl ether identified with *.

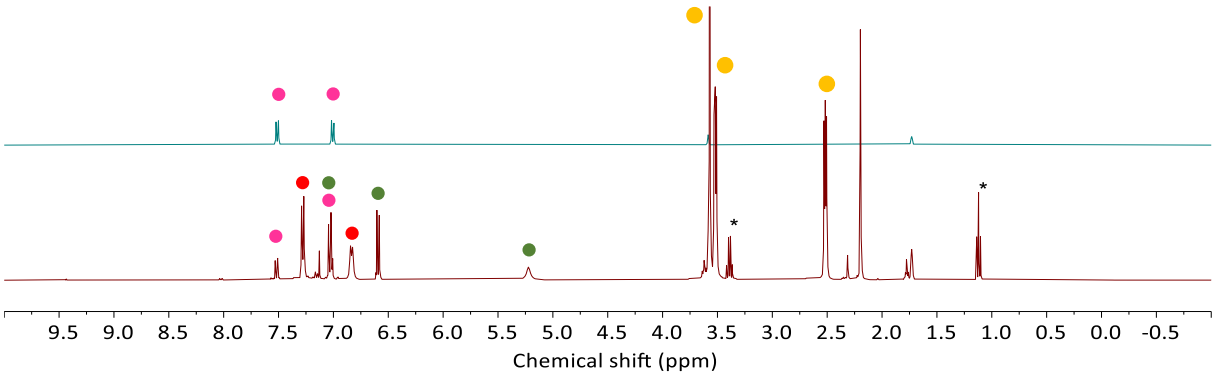

Figure S34: Stacked ^{1}H NMR spectra (400 MHz, THF-d_8) of 4-$BrC_6H_4N_3$ (top) and the reaction mixture 3.3.1 (bottom).

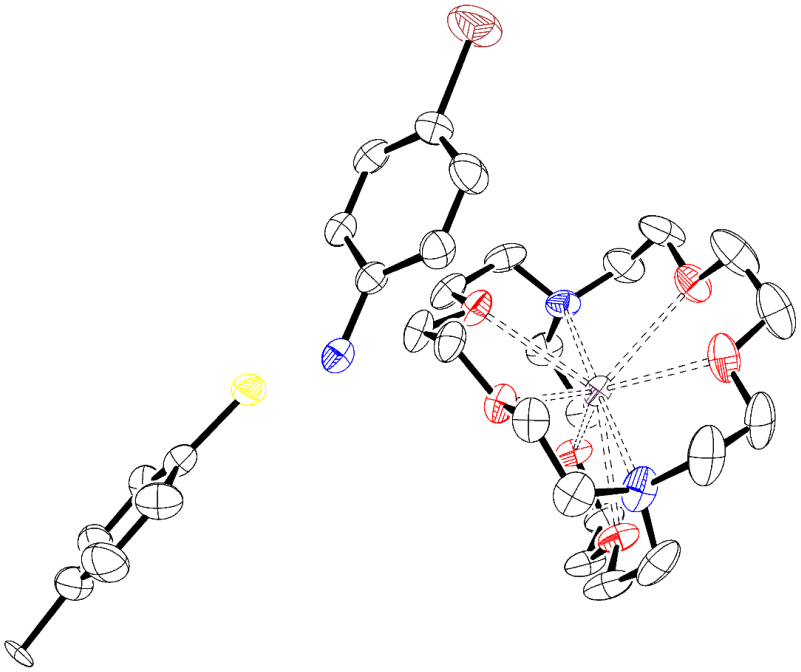

Figure S35: Molecular structure of [K(crypt)][**4**] + **6** showing anisotropic displacement ellipsoids at 50% probability with hydrogen atoms omitted for clarity. Nitrogen: blue; carbon: white; bromine: brown; sulfur: yellow; oxygen: red; potassium: violet.

3.3.2 Addition of 4 equivalents of TolSH

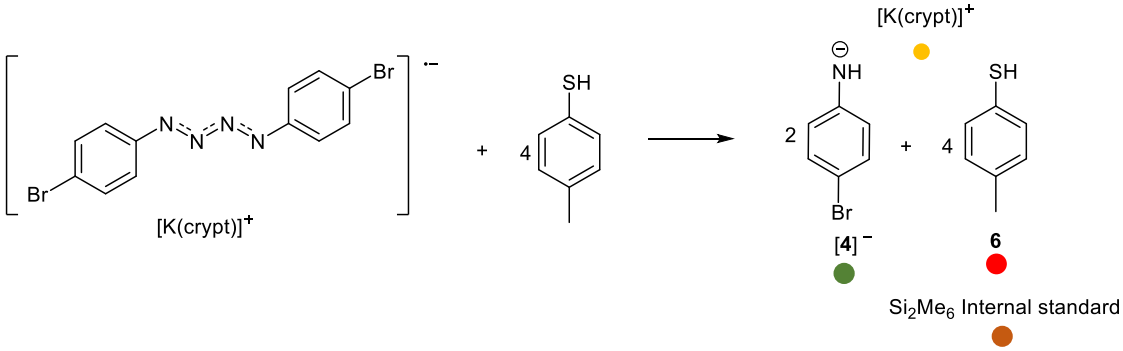

In the glovebox, a solution of TolSH (12.7 mg, 0.102 mmol, 4 equiv.) in THF (1 mL) was added to a vial containing [K(crypt)][**1**] (18.8 mg, 0.023 mmol, 1 equiv.). The solution was shaken for 1 minute before removing the solvent under vacuum. The remaining solid was washed with ether and dried under vacuum before analyzing by NMR spectroscopy in THF-d_8 (0.5 mL). Single crystals from the reaction were obtained via slow diffusion of hexane into the reaction mixture and [K(crypt)][**4**] + **6** was again observed by XRD. EPR spectrometry was conducted on the reaction mixture and no resonances were observed, confirming the presence of only diamagnetic products.

NMR conversion: 64% (amine integration vs. Si_2Me_6 internal standard)

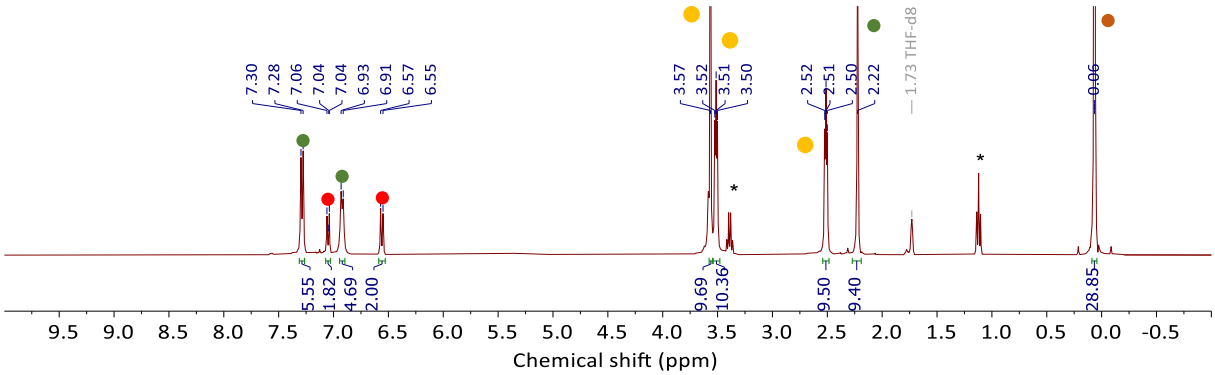

Figure S36: ^{1}H NMR spectrum (400 MHz, THF-d_8) of [K(crypt)][**4**] + **6** after work-up. Circles above signals identify the products and dimethyl ether identified with *.

3.3.3 Independent preparation of 1:2 mixture of [K(crypt)][**4**] + **6**.

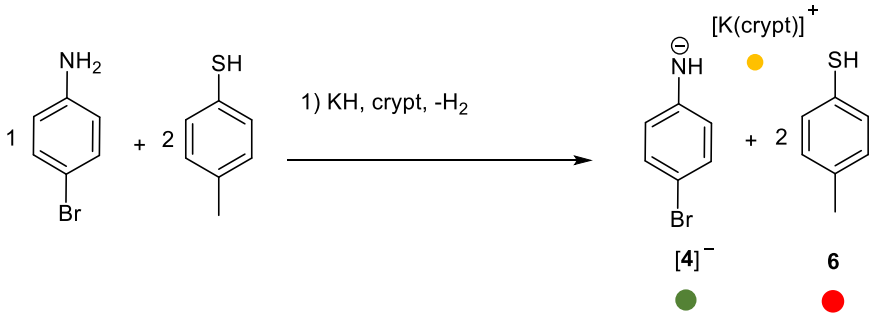

In order to confirm the presence of [K(crypt)][**4**] + **6** in the reactions with TolSH, a mixture of K(crypt)][**4**] + **6** was independently prepared and used to compare reaction mixture NMR data. In a vial, 4-bromoaniline (20.0 mg, 0.012 mmol, 1 equiv.), cryptand-2.2.2 (43.6 mg, 0.012 mmol, 1 eqv.) and TolSH (28.8 mg, 0.024 mmol, 2 equiv.) were dissolved in THF-d_8 (0.5mL). Potassium hydride (4.7 mg, 0.012 mmol, 1 equiv.) was added and shaken for 1 minute with gas evolution being observed. The mixture was then filtered into a J Young NMR tube for analysis. Broadening of the aromatic signals and changing of their chemical shift depends on the ratio [**4**]$^-$:**6** is consistent with a proton on the thiol shuttling between the sulfur and the nitrogen of the amide. This is consistent with XRD data for [K(crypt)][**4**] + **6**, where the potassium is found between the two compounds and the nitrogen and sulfur atoms point towards one another.

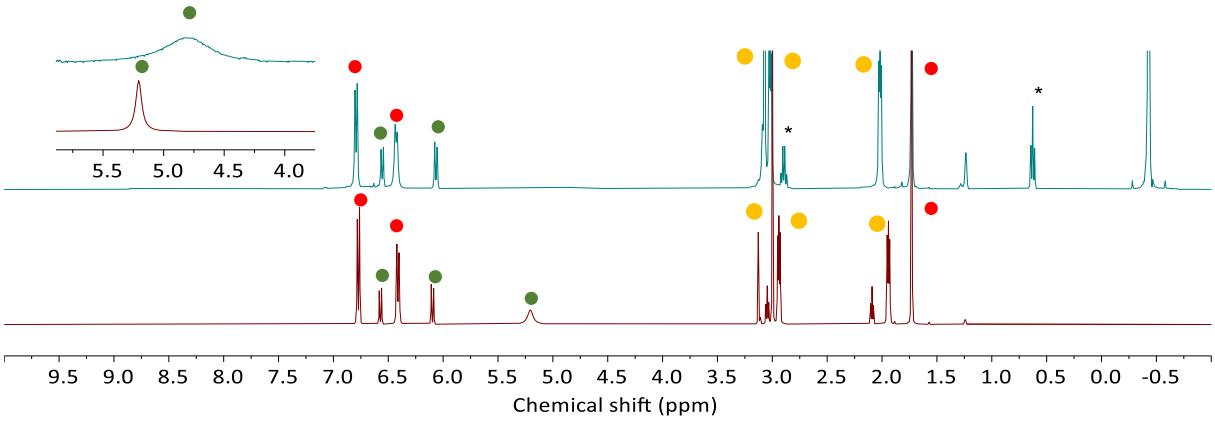

Figure S37: Stacked ^{1}H NMR spectra (400 MHz, THF-d_8) of reaction mixture 3.3.2 (top) and independently prepared 2:1 mixture [K(crypt)][**4**] + **6** (bottom) with an inset showing the labile proton. Circles above signals identify the products and diethyl ether identified with *.

3.4 Reaction with 4-IC$_6$H$_4$CHO

3.4.1. Reaction in THF-d_8 and crude NMR spectra

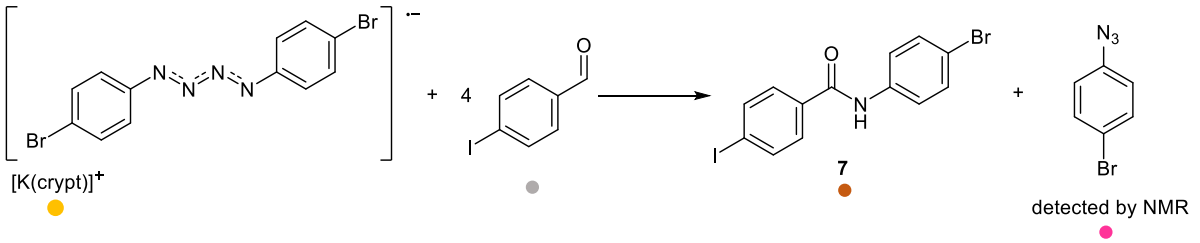

In a glovebox, [K(crypt)][**1**] (60 mg, 0.0765 mmol, 1 equiv.) and 4-iodobenzaldehyde (72 mg, 0.306 mmol, 4 equiv.) were dissolved in THF-d_8 and a crude NMR taken immediately to identify the fate of the remaining atoms in [K(crypt)][**1**] that were not observed in product **7**. 4-BrC$_6$H$_4$N$_3$ could be observed in the crude reaction mixture NMR spectra.

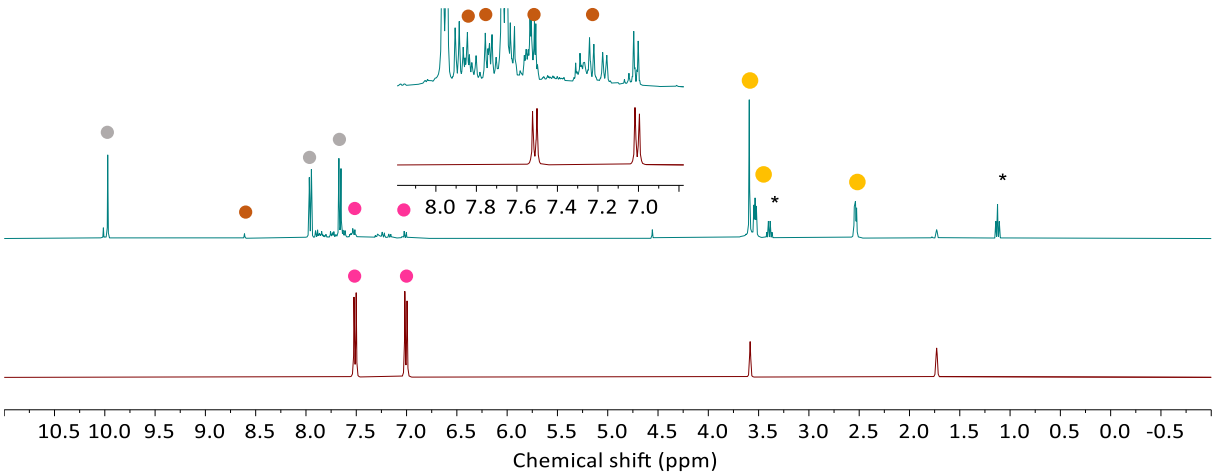

Figure S38: ^{1}H NMR spectra (400 MHz, THF-d_8) of the crude reaction mixture between [K(crypt)][**1**] and 4 equivalents of 4-iodobenzaldehyde (top) stacked with 4-Br$C_6H_4N_3$ (bottom) with an inset zoomed into the aromatic region. Circles above signals identify the products and diethyl ether identified with *.

3.4.2. Reaction in *o*DFB and isolation of **7**

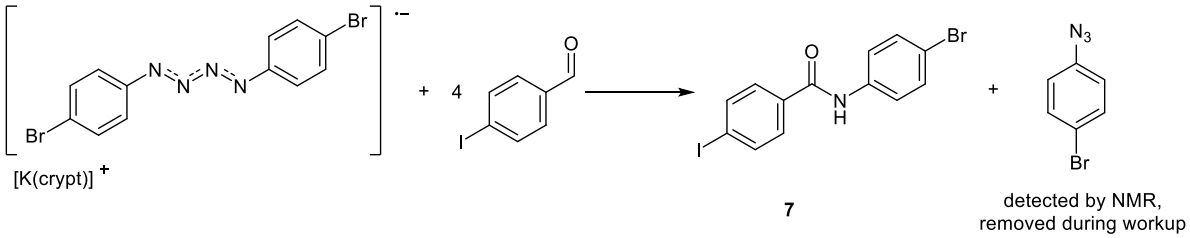

In a glovebox, [K(crypt)][**1**] (60 mg, 0.0765 mmol, 1 equiv.) and 4-iodobenzaldehyde (72 mg, 0.306 mmol, 4 equiv.) were dissolved in *o*DFB (2 mL) and stirred for 2 hours. The solvent was removed in vacuo yielding a dark red oil which was extracted with ether and passed through a silica plug using chloroform. The solvent was then removed and excess 4-iodobenzaldehyde removed by vacuum distillation at 45 °C yielding compound **7**.

Isolated Yield: 20.2 mg (66%)

Mass Spectrometry: $[M-H]^-$ Found 399.8843 Calculated 399.8839

^{1}H NMR (400 MHz, 298 K, $CDCl_3$): δ = 8.36 (s, 1H, N*H*), 7.83 (d, 2H, $^{3}J_{H-H}$ = 8.4 Hz, Ar), 7.62 (d, 2H, $^{3}J_{H-H}$ = 8.4 Hz, Ar), 7.51 (d, 2H, $^{3}J_{H-H}$ = 8.7 Hz, Ar), 7.09 (d, 2H, $^{3}J_{H-H}$ = 8.7f Hz, Ar).

^{13}C{^{1}H} NMR (101 MHz, 298 K, $CDCl_3$): δ = 159.53 (s, *C*=O), δ = 138.10 (s, Ar), δ = 137.72 (s, Ar), δ = 135.40 (s, Ar), δ = 132.28 (s, Ar), δ = 130.24 (s, Ar), δ = 129.25 (s, Ar), δ = 122.57 (s, Ar), δ = 98.59 (s, Ar),

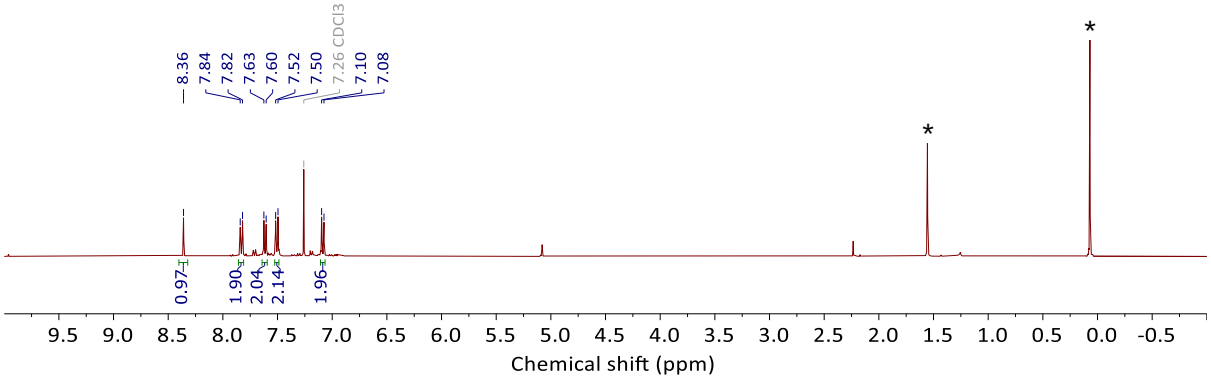

Figure S39: ^{1}H NMR spectrum (400MHz, $CDCl_3$) of compound **7** (* indicates water and TMS in bench stored $CDCl_3$).

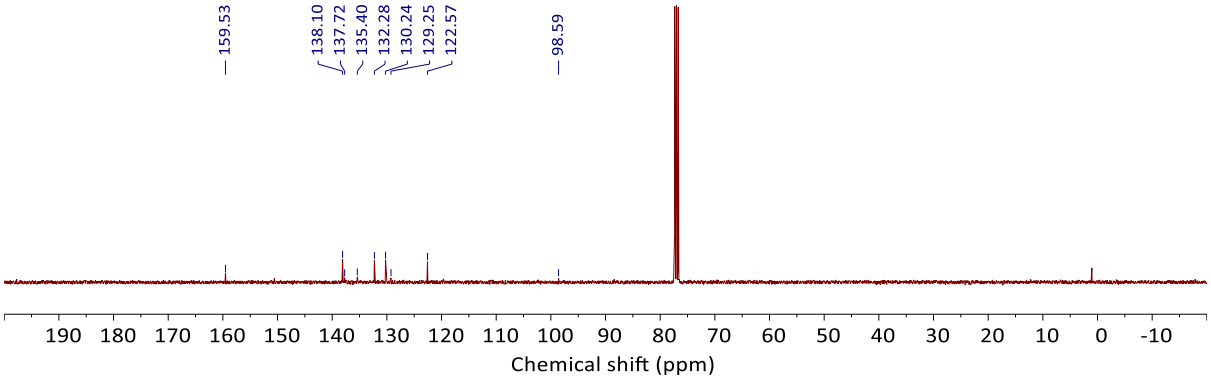

Figure S40: ^{13}C{1H} NMR spectrum (101 MHz, $CDCl_3$) of compound **7**.

3.4.3. Control reaction of 4-BrPhNHK with 4-IC_6H_4CHO

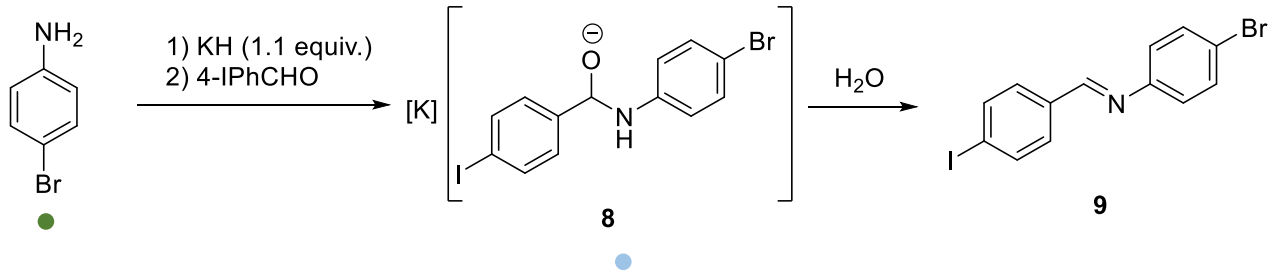

In a glovebox, 4-bromoaniline (15.2mg, 0.125 mmol, 1 equiv.) and potassium hydride (5.5mg, 0.138, 1.1 equiv.) were stirred in THF for 30 minutes. The reaction mixture was filtered and 4-IC_6H_4CHO (29 mg, 0.125 mmol, 1 equiv.) was added. The reaction mixture was filtered into a J Young NMR tube and analyzed by NMR spectroscopy yielding compound **8**. Mass spectrometry was conducted on **8** with the major peak being of **9**, the expected product of the dehydration of **8**. Water was added to **8**, filtered and dried in vacuo. The resultant yellow solid was analyzed by NMR spectroscopy and the product was determined to be **9**. It is worth noting that intermediates related to **8** have been previously reported when aldehydes are converted to imines.[33, 34]

Isolated Yield (**9**): 75% (36.1 mg)

NMR data of compound **8**:

^{1}H NMR (400 MHz, 298 K, THF): δ= 8.44 (s, 1H, *H*CON), 7.82 (d, 2H, $^{2}J_{H\text{-}H}$ = 8.2 Hz Ar), 7.64 (d, 2H, $^{2}J_{H\text{-}H}$ = 8.2 Hz Ar), 7.48 (d, 2H, $^{2}J_{H\text{-}H}$ = 8.8 Hz Ar), 7.12 (d, 2H, $^{2}J_{H\text{-}H}$ = 8.8 Hz Ar), 4.71 (s, 1H, N*H*).

NMR data of compound **9**:

^{1}H NMR (400 MHz, 298 K, $CDCl_3$): δ= 8.36 (s, 1H, *H*CN), 7.83 (d, 2H, $^{2}J_{H\text{-}H}$ = 8.2 Hz Ar), 7.62 (d, 2H, $^{2}J_{H\text{-}H}$ = 8.2 Hz Ar), 7.51 (d, 2H, $^{2}J_{H\text{-}H}$ = 8.8 Hz Ar), 7.09 (d, 2H, $^{2}J_{H\text{-}H}$ = 8.8 Hz Ar).

Mass Spectrometry: [**9**+H]$^{+}$ Found 385.9035 Calculated 385.9036

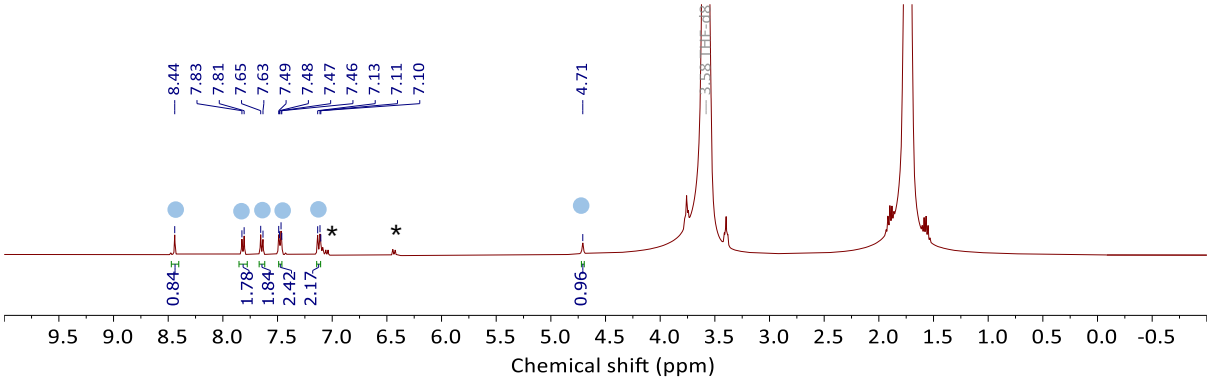

Figure S41: ^{1}H NMR spectrum (400MHz, THF) of compound **8** with unreacted 4-BrPhNHK marked with *.

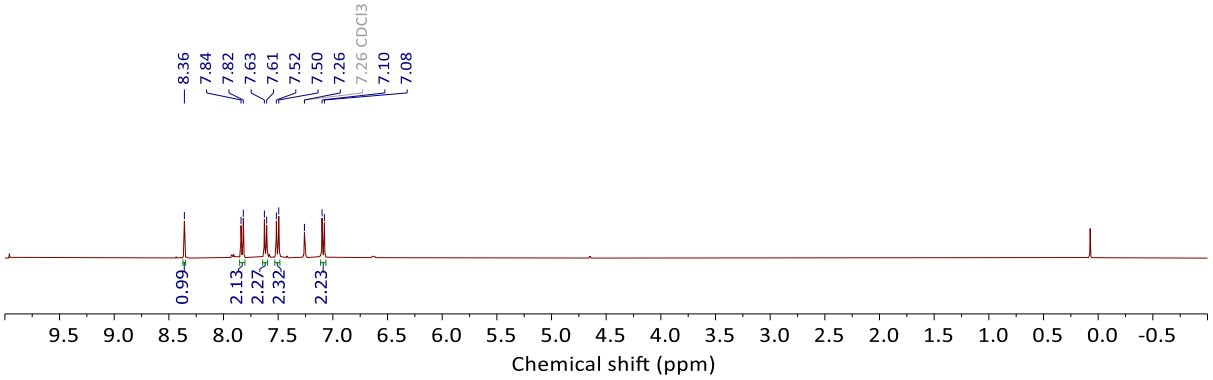

Figure S42: ^{1}H NMR spectrum (400MHz, $CDCl_3$) of isolated compound **9.**

3.5 Calculated Energy of Azide Loss

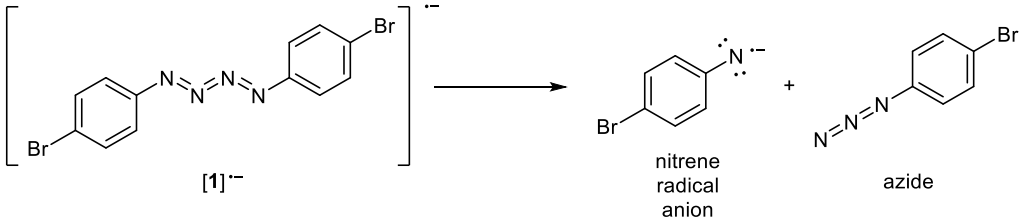

Table S9: Calculated electronic and Gibbs energies for the production of a radical anion and azide from [**1**]•−

Solvent	ΔE (kcal/mol)	ΔG (kcal/mol)
THF	36.7	19.2
Cyclopentanone	36.3	19.3

4. Crystallography Tables

Identification code	**[K(crypt)][1]**	**$[K(THF_2)]_2$[2]**
Empirical formula	$C_{15}H_{22}BrK_{0.5}N_3O_3$	$C_{14}H_{20}BrKN_2O_2$
Formula weight	391.81	367.33
Temperature/K	99.9(3)	150.00(10)
Crystal system	monoclinic	monoclinic
Space group	C2/c	$P2_1/c$
a/Å	25.6890(5)	5.6891(4)
b/Å	8.1881(2)	14.7673(5)
c/Å	20.2875(5)	19.7659(6)
α/°	90	90
β/°	98.540(2)	96.186(4)
γ/°	90	90
Volume/$Å^3$	4220.04(17)	1650.92(14)
Z	8	4
$\rho_{calc}g/cm^3$	1.233	1.478
μ/mm^{-1}	3.658	5.676
F(000)	1612.0	752.0
Crystal size/mm^3	0.245 × 0.091 × 0.054	0.399 × 0.172 × 0.079
Radiation	Cu Kα (λ = 1.54184)	Cu Kα (λ = 1.54184)
2Θ range for data collection/°	6.96 to 152.788	7.488 to 153.042
Index ranges	-32 ≤ h ≤ 32, -10 ≤ k ≤ 10, -25 ≤ l ≤ 25	-7 ≤ h ≤ 7, -18 ≤ k ≤ 18, -18 ≤ l ≤ 24
Reflections collected	47401	18039
Independent reflections	4384 [R_{int} = 0.0758, R_{sigma} = 0.0284]	3427 [R_{int} = 0.0483, R_{sigma} = 0.0310]
Data/restraints/parameters	4384/373/262	3427/573/291
Goodness-of-fit on F^2	1.157	1.054
Final R indexes [I>=2σ (I)]	R_1 = 0.0706, wR_2 = 0.2019	R_1 = 0.0464, wR_2 = 0.1175
Final R indexes [all data]	R_1 = 0.0730, wR_2 = 0.2035	R_1 = 0.0616, wR_2 = 0.1327
Largest diff. peak/hole / e $Å^{-3}$	0.69/-1.28	0.49/-0.58
CCDC	2423978	2423981

Identification code	**3**	**[K(crypt)][4] + 6**
Empirical formula	$C_{36}H_{30}Sn_2$	$C_{31}H_{49}BrKN_3O_6S$
Formula weight	699.98	710.80
Temperature/K	150.00(10)	150.00(10)
Crystal system	monoclinic	orthorhombic
Space group	$P2_1/n$	Pbca
a/Å	17.0537(3)	23.3381(2)
b/Å	9.27280(10)	27.1976(3)
c/Å	20.2706(3)	11.35040(10)
α/°	90	90
β/°	111.898(2)	90
γ/°	90	90
Volume/Å^3	2974.22(8)	7204.56(12)
Z	4	8
ρ_{calc}g/cm^3	1.563	1.311
μ/mm^{-1}	13.510	3.479
F(000)	1384.0	2992.0
Crystal size/mm^3	0.266 × 0.207 × 0.121	0.328 × 0.277 × 0.105
Radiation	Cu Kα (λ = 1.54184)	Cu Kα (λ = 1.54184)
2Θ range for data collection/°	8.54 to 152.302	7.576 to 152.642
Index ranges	-21 ≤ h ≤ 21, -10 ≤ k ≤ 11, -25 ≤ l ≤ 21	-29 ≤ h ≤ 29, -34 ≤ k ≤ 31, -14 ≤ l ≤ 14
Reflections collected	15884	154596
Independent reflections	6166 [R_{int} = 0.0327, R_{sigma} = 0.0322]	7536 [R_{int} = 0.0604, R_{sigma} = 0.0150]
Data/restraints/parameters	6166/0/343	7536/0/389
Goodness-of-fit on F^2	1.035	1.161
Final R indexes [I>=2σ (I)]	R_1 = 0.0370, wR_2 = 0.0984	R_1 = 0.0871, wR_2 = 0.2171
Final R indexes [all data]	R_1 = 0.0390, wR_2 = 0.1003	R_1 = 0.0884, wR_2 = 0.2177
Largest diff. peak/hole / e Å^{-3}	3.48/-1.35	1.04/-1.47
CCDC	2423980	2423979

Justification for B alert in **3**.

PLAT971_ALERT_2_B Check Calcd Resid. Dens. 1.70Ang From Sn02 3.33 eA-3

Author Response: Residual electron density is observed around the heavy Sn atom.

5. References

1. Heurich T, Nesterov V, Schnakenburg G, Qu Z-W, Grimme S, Hazin K*, et al.* Strong Evidence of a Phosphanoxyl Complex: Formation, Bonding, and Reactivity of Ligated Phosphorus Analogues of Nitroxides. *Angew. Chem. Int. Ed.* 2016, **55**(46)**:** 14439–14443.

2. Maier TM, Coburger P, van Leest NP, Hey-Hawkins E, Wolf R. Direct Synthesis of an Anionic 13-Vertex Closo-Cobaltacarborane Cluster. *Dalton Trans.* 2019, **48**(42)**:** 15772–15777.

3. Stoll S, Schweiger A. EasySpin, A Comprehensive Software Package for Spectral Simulation and Analysis in EPR. *J. Magn. Reson.* 2006, **178**(1)**:** 42–55.

4. CrysAlis PRO. Agilent Technologies Ltd: Yarnton O, England 2014.

5. Sheldrick G. SHELXT - Integrated Space-Group and Crystal-Structure Determination. *Acta Crystallogr. A* 2015, **71**(1)**:** 3–8.

6. Dolomanov OV, Bourhis LJ, Gildea RJ, Howard JAK, Puschmann H. OLEX2: A Complete Structure Solution, Refinement and Analysis Program. *J. Appl. Cryst.* 2009, **42:** 339–341.

7. Kabova EA, Blundell CD, Muryn CA, Whitehead GFS, Vitorica-Yrezabal IJ, Ross MJ*, et al.* SDPD-SX: Combining a Single Crystal X-Ray Diffraction Setup with Advanced Powder Data Structure Determination for Use in Early Stage Drug Discovery. *CrystEngComm* 2022, **24**(24)**:** 4337–4340.

8. Coelho A. An Indexing Algorithm Independent of Peak Position Extraction for X-ray Powder Diffraction Patterns. *J. Appl. Crystallogr.* 2017, **50**(5)**:** 1323–1330.

9. Petříček V, Dušek M, Palatinus L. Crystallographic Computing System JANA2006: General features. *Z. Kristallogr. Cryst. Mater.* 2014, **229**(5)**:** 345–352.

10. Frisch MJ, Trucks GW, Schlegel HB, Scuseria GE, Robb MA, Cheeseman JR*, et al.* Gaussian 16 Rev. C.01. Wallingford, CT; 2016.

11. Tao J, Perdew JP, Staroverov VN, Scuseria GE. Climbing the Density Functional Ladder: Nonempirical Meta--Generalized Gradient Approximation Designed for Molecules and Solids. *Phys. Rev. Lett.* 2003, **91**(14)**:** 146401.

12. Grimme S. Supramolecular Binding Thermodynamics by Dispersion-Corrected Density Functional Theory. *Chem. Eur. J.* 2012, **18**(32)**:** 9955–9964.

13. Luchini G, Alegre-Requena J, Funes-Ardoiz I, Paton R. GoodVibes: Automated Thermochemistry for Heterogeneous Computational Chemistry Data. *F1000Research* 2020, **9**(291).

14. Weigend F, Ahlrichs R. Balanced Basis Sets of Split Valence, Triple Zeta Valence and Quadruple Zeta Valence Quality for H to Rn: Design and Assessment of Accuracy. *Phys. Chem. Chem. Phys.* 2005, **7**(18)**:** 3297–3305.

15. Marenich AV, Cramer CJ, Truhlar DG. Universal Solvation Model Based on Solute Electron Density and on a Continuum Model of the Solvent Defined by the Bulk Dielectric Constant and Atomic Surface Tensions. *J. Phys. Chem. B* 2009, **113**(18)**:** 6378–6396.

16. NBO 7.0. E. D. Glendening J, K. Badenhoop, A. E. Reed, J. E. Carpenter, J. A. Bohmann, C. M. Morales, P. Karafiloglou, C. R. Landis, and F. Weinhold, Theoretical Chemistry Institute, University of Wisconsin, Madison (2018).

17. Staroverov VN, Scuseria GE, Tao J, Perdew JP. Comparative Assessment of a New Nonempirical Density Functional: Molecules and Hydrogen-Bonded Complexes. *J. Chem. Phys.* 2003, **119**(23)**:** 12129–12137.

18. Neese F. The ORCA program system. *WIREs Computational Molecular Science* 2012, **2**(1)**:** 73–78.

19. Becke AD. Density-Functional Thermochemistry. III. The Role of Exact Exchange. *J. Chem. Phys.* 1993, **98**(7)**:** 5648–5652.

20. Lee C, Yang W, Parr RG. Development of the Colle-Salvetti Correlation-Energy Formula into a Functional of the Electron Density. *Phys. Rev. B* 1988, **37**(2)**:** 785–789.

21. Kendall RA, Dunning TH, Jr., Harrison RJ. Electron Affinities of the First-Row Atoms Revisited. Systematic Basis Sets and Wave Functions. *J. Chem. Phys.* 1992, **96**(9)**:** 6796–6806.

22. Barone V. Structure, Magnetic Properties and Reactivities of Open-Shell Species From Density Functional and Self-Consistent Hybrid Methods. *Recent Advances in Density Functional Methods*, pp 287–334.

23. Hassan I, Pavlov J, Errabelli R, Attygalle AB. Oxidative Ionization Under Certain Negative-Ion Mass Spectrometric Conditions. *J. Am. Soc. Mass Spectrom.* 2017, **28**(2)**:** 270–277.

24. Perdew JP, Burke K, Ernzerhof M. Generalized Gradient Approximation Made Simple. *Phys. Rev. Lett.* 1996, **77**(18)**:** 3865–3868.

25. Adamo C, Barone V. Toward Reliable Density Functional Methods Without Adjustable Parameters: The PBE0 Model. *J. Chem. Phys.* 1999, **110**(13)**:** 6158–6170.

26. Chai J-D, Head-Gordon M. Long-Range Corrected Hybrid Density Functionals with Damped Atom–Atom Dispersion Corrections. *Phys. Chem. Chem. Phys.* 2008, **10**(44)**:** 6615–6620.

27. Bain GA, Berry JF. Diamagnetic Corrections and Pascal's Constants. *J. Chem. Educ.* 2008, **85**(4)**:** 532.

28. Gulaczyk I, Kręglewski M, Valentin A. The N–N Stretching Band of Hydrazine. *J. Mol. Spectrosc.* 2003, **220**(1)**:** 132–136.

29. Fujino T, Tahara T. Picosecond Time-Resolved Raman Study of trans-Azobenzene. *J. Phys. Chem. A* 2000, **104**(18)**:** 4203–4210.

30. Yanai T, Tew DP, Handy NC. A New Hybrid Exchange–Correlation Functional using the Coulomb-Attenuating Method (CAM-B3LYP). *Chem. Phys. Lett.* 2004, **393**(1)**:** 51–57.

31. Wang Y, Verma P, Jin X, Truhlar DG, He X. Revised M06 Density Functional for Main-Group and Transition-Metal Chemistry. *Proc. Natl. Acad. Sci.* 2018, **115**(41)**:** 10257–10262.

32. Dainis Dakternieks, Fong Sheen Kuan, Andrew Duthie, Edward R. T. Tiekink. The Crystal Structure of the Triclinic Polymorph of Hexaphenyldistannane. *Main Group Met. Chem.* 2001, **24**(1)**:** 65–66.

33. Ding Y-G, Cui Y-Z, Li T-D. New Views on the Reaction of Primary Amine and Aldehyde from DFT Study. *J. Phys. Chem. A* 2015, **119**(18)**:** 4252–4260.

34. Kwiecień A, Ciunik Z. Stable Hemiaminals: 2-Aminopyrimidine Derivatives. *Molecules*; 2015. pp. 14365–14376.